Petrology, petrogenesis, and geochronology review of the Cenozoic adakitic rocks of northeast Iran: Implications for evolution of the northern branch of Neo-Tethys

Fazilat Yousefi[1] | Mahmoud Sadeghian[1] | David R. Lentz[2] |
Christina Wanhainen[3] | Ryan D. Mills[4]

[1]Faculty of the Earth Science, Shahrood University of Technology, Shahrood, Iran

[2]Department of Earth Sciences, University of New Brunswick, Fredericton, New Brunswick, Canada

[3]Department of Civil, Environmental and Natural Resources Engineering, Lulea University of Technology, Lulea, Sweden

[4]Department of Geological Sciences, University of North Carolina at Chapel Hill, Chapel Hill, North Carolina

Correspondence
Fazilat Yousefi, Faculty of the Earth Science, Shahrood University of Technology, Shahrood, Iran.
Email: f.yousefi87@gmail.com

Cenozoic adakitic rocks of the northern part of the Central Iran Structural Zone (CISZ) are among the notable geological features of the terrains in northeast Iran, so a comprehensive comparison of several of these adakitic sequences is presented. This lithogeochemical analysis is constrained to examining adakitic magmatism of the three magmatic belts within the CISZ, which from southeast to northeast and from oldest to youngest are as follows: (a) south of Shahrood-Damghan, (b) north-northwest of Sabzevar-Neyshabour, and (c) south of Qouchan and west of Esfarayen. Radiogenic isotope analysis using Rb–Sr and Sm–Nd methods show that the adakitic rocks associated with Qouchan-Esfarayen magmatism have 0.512581 to 0.51288 initial ^{143}Nd/^{144}Nd and 0.703903 to 0.705627 initial ^{87}Sr/^{86}Sr, with εNd -0.86 to 4.98. Adakitic rocks in south to southeast Shahrood have 0.512775 to 0.512893 initial ^{143}Nd/^{144}Nd and 0.703746 to 0.705314 initial ^{87}Sr/^{88}Sr, with εNd 3.69 to 6.0, and adakites emplaced into the Sabzevar ophiolite have 0.512846 to 0.512911 initial ^{143}Nd/^{144}Nd and 0.70379 to 0.705019 initial ^{87}Sr/^{86}Sr contents with εNd of 5.26 to 6.54. Isotopic initial ratios of Nd and Sr support an origin involving partial melting of the subducting oceanic lithosphere of the northern branch of Neo-Tethys and the associated suprasubduction mantle wedge in producing these adakitic rocks.

KEYWORDS

central iran structural zone, adakite, Cenozoic, Iran, slab melting

1 | INTRODUCTION

There are many reports of Cenozoic magmatic activity (Palaeocene to Quaternary) in Iran. Geological maps illustrate the distribution of magmatism, reflecting the importance of Cenozoic magmatism in the region (Haghipour & Aghanabati, 1985; Yousefi, Sadeghian, Samyari, & Ghasemi, 2017). Also Maghdour-Mashhour, Esmaeily, Shabani, Chiaradia, and Latypov (2015) have pointed to volcanic and plutonic rocks that outcrop in central (Urumieh–Dokhtar Magmatic Assemblage, UDMA) and north–northeastern Iran (Alborz Magmatic Belt, AMB); they proposed that this magmatism marked the beginning of subduction of the Neo-Tethyan oceanic lithosphere beneath the south–southwestern border of the Turkish–Iranian high plateau and was

approximately simultaneous with the closure of Palaeotethys in southern Eurasia during the Late Permian–Early Triassic. In several parts of the Central Iran Structural Zone (CISZ), there are numerous intrusions with intermediate to felsic compositions with adakitic geochemical signatures (Gardideh, Ghasemi, & Sadeghian, 2018; Jamshidi, Ghasemi, Miao, & Sadeghian, 2018; Jamshidi, Ghasemi, Troll, Sadeghian, & Dahren, 2015; Yousefi et al., 2017).

Adakite was first introduced by Kay (1978) and then Defant and Drummond (1990) as a specific group of rocks that are of intermediate to felsic compositions, formed in an arc setting withspecific geochemical characteristics of $SiO_2 \geq 56$ wt%, high Na_2O contents (3.5 wt% $\leq Na_2O \leq 7.5$ wt%), and high La/Yb > 40 and Sr/Y ratios, with a strong depletion in certain high-field-strength elements (HFSE), especially heavy

rare earth elements (HREE) (Yb) and Y, and with low $^{87}Sr/^{86}Sr$ initial ratios. Martin, Smithies, Rapp, Moyen, and Champion (2005) suggested that adakites can be subdivided into two subcategories, that is, high silica adakite (HSA) and low silica adakite (LSA). According to Moyen and Stevens (2006) and Deng et al. (2017), original adakitic rocks were the result of partial melting of metabasaltic rocks at relatively high pressure, with eclogites or amphibolites in the residua. Ribeiro, Maury, and Grégoire (2016) have stated that adakites are unusual felsic igneous rocks commonly associated with asthenospheric slab window opening or fast subduction of a young (hot) oceanic plate that may allow slab melting at shallow depths. One of the most interesting features of the adakitic rocks is the mineralization potential (porphyry Cu–Au) of these intrusives and as such there is considerable interest in their range of petrogeneses. Simmonds (2013) conducted a study of mineralization along with adakitic rocks in the Kighal area, northwest Iran. He has identified these adakitic rocks as modern adakites, which are associated with Cu–Au
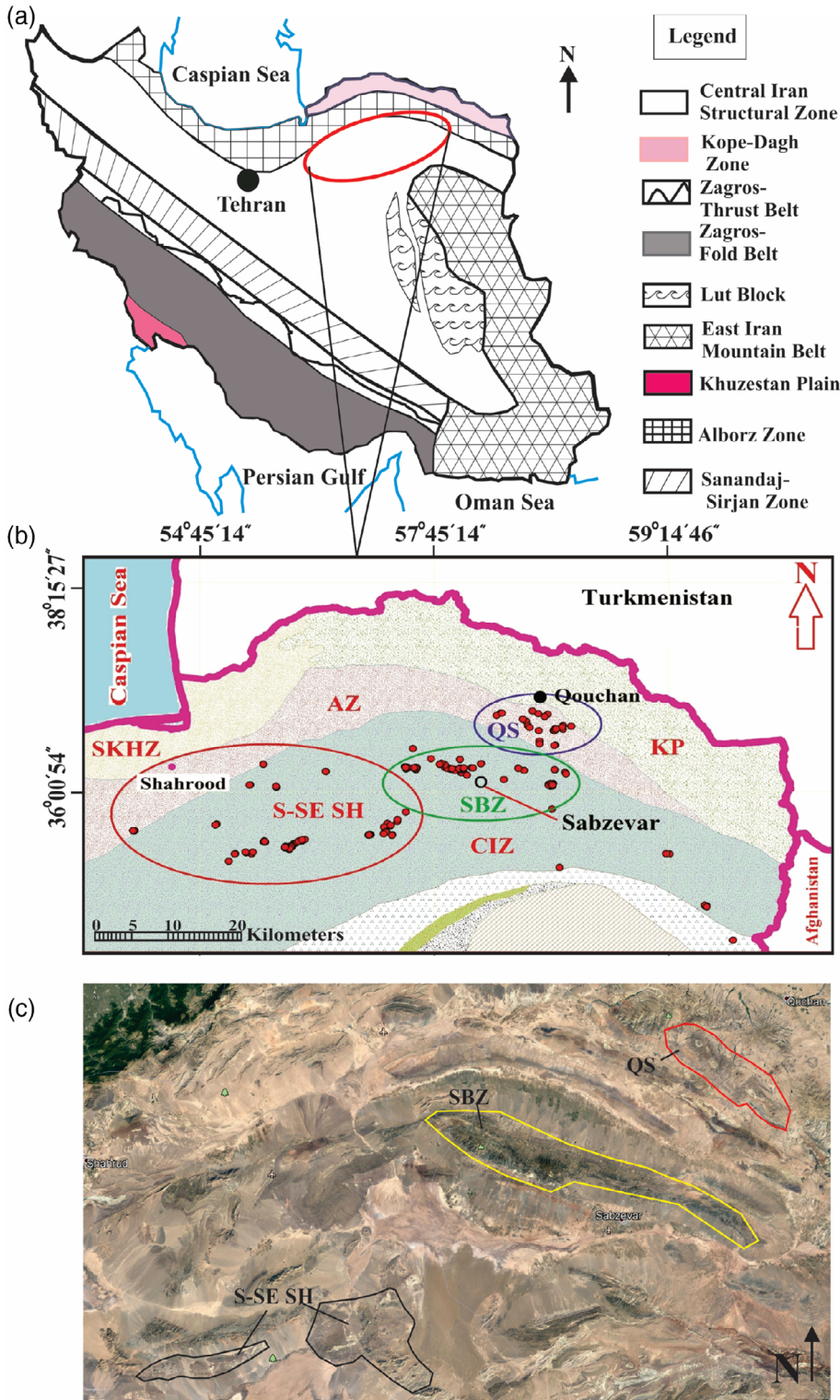

FIGURE 1   Location map showing the main structural zone of northeast of Iran and distribution of adakitic dikes, domes, plutons, and pyroclastic rocks, which penetrated or are associated with rocks by interval range from Late Neoproterozoic up to Late Miocene, but mainly intruding in Late Cretaceous–Early Palaeocene ophiolitic rocks (related to closure of Sabzevar Neo-Tethys branch) and north of Central Iran Structural Zone Eocene-Miocene magmatic belt. Most of the adakitic rocks have less than 2 km^2 extent, so we prefer to show them by points on the large-scale maps. Abbreviation signs in the figure (b) includes: AZ: Alborz, SKHZ: Khazar-Talesh-Ziveh structural zone, KP: Kopeh Dagh, CIZ: Central Iran zone, QS: Qouchan-Esfarayen, S-SE SH: South-Southeast of Shahrood, SBZ: Sabzevar. The areas of magmatic belts of each section are shown in part (c) of figure [Colour figure can be viewed at wileyonlinelibrary.com]

mineralization. These adakitic rocks are thought to be the result of subduction of the Neo-Tethys Oceanic plate. According to surveys by du Bray (2017), igneous rocks and epithermal deposits, such as Au and Ag producing systems, have a close spatial and temporal association with each other and commonly have a genetic relationship with adakitic stocks and dykes and related volcanic rocks. He also presented evidence that deposit formation depends on optimization of source metals (Cu, Au, Ag) contents, appropriate fluid compositions, and characteristic structural features.

Adakitic rocks in northeast Iran usually are exposed as dikes, small outcrops representing hypabyssal domes, and small intrusions (stocks to plutons) (Figure 1). The specific focus of this analysis is magmatism in the northern part of the CISZ, which includes smaller magmatic belts, such as Torud–Ahmad Abad, Abbas Abad–Davarzan-Sabzevar, and Qouchan–Esfarayen (Yousefi, 2017; Yousefi, Sadeghian, Samyari, & Ghasemi, 2017). These areas have also been mentioned by Jamshidi et al. (2015) and Gardideh et al. (2018), where recent research has been carried out in these regions as well.

Hypabyssal rocks in the northern CISZ have been emplaced into the older Eocene volcanic and volcano-sedimentary rocks. These Middle Eocene to Miocene–Pliocene igneous rocks are evidence of subduction of the Sabzevar branch of the Neo-Tethys Ocean. The association of these hypabyssal magmatic rocks and melting Neo-Tethys oceanic plate has been widely accepted by researchers (Ghasemi & Rezaei Kahkhaei, 2015; Jamshidi et al., 2015; Yousefi, Sadeghian, Samyari, & Ghasemi, 2017; Yousefi, Sadeghian, Wanhainen, et al., 2017). According to geothermobarometry of some phenocrysts, such as amphibole, plagioclase, and pyroxene, in these adakites in some of these regions, the depth of the beginning of magma crystallization (before shallow emplacement) is estimated to be <30 km (Jamshidi et al., 2015; Yousefi, Sadeghian, Wanhainen, et al., 2017). Our focus is on the three neighbouring areas, where magmatism occurred, that is, Sabzevar, Qouchan-Esfarayen, and south to southeast Shahrood. This survey is based on comparing geochemical evidence, isotope systematics, and robust geochronology so as to enhance the petrogenetic and geodynamic interpretation of these key igneous systems.

2 | GEOLOGICAL SETTING AND ROCK TYPES

2.1 | Geological setting and field relation

The formation of these magmatic belts in this part of Central Iran is due to the convergence of Arabian and Eurasian plates. According to Molinaro, Zeyen, and Laurencin (2005), the Zagros Mountains are a young, active collisional belt developed at the frontier between the converging Arabian and Eurasian plates. Maghdour-Mashhour et al. (2015) and Verdel, Wernicke, Hassanzadeh, and Guest (2011) found that the rate of plate convergence has reduced from ~6–7 cm/yr in the Middle to Late Cretaceous to relatively slow values of 3–3.5 cm/yr during the latest Cretaceous, which persisted through the Eocene. Berberian and Berberian (1981) noted that tectonic activity in Iran included several stages of deformation with one of the most important stages being the tectonic events of the Neo-Tethys oceanic plate after the Late Carboniferous. Neo-Tethys closure occurred during the Mesozoic and Cenozoic. The closure of the Palaeo-Tethys Ocean occurred in the Triassic by movement to the north of the central
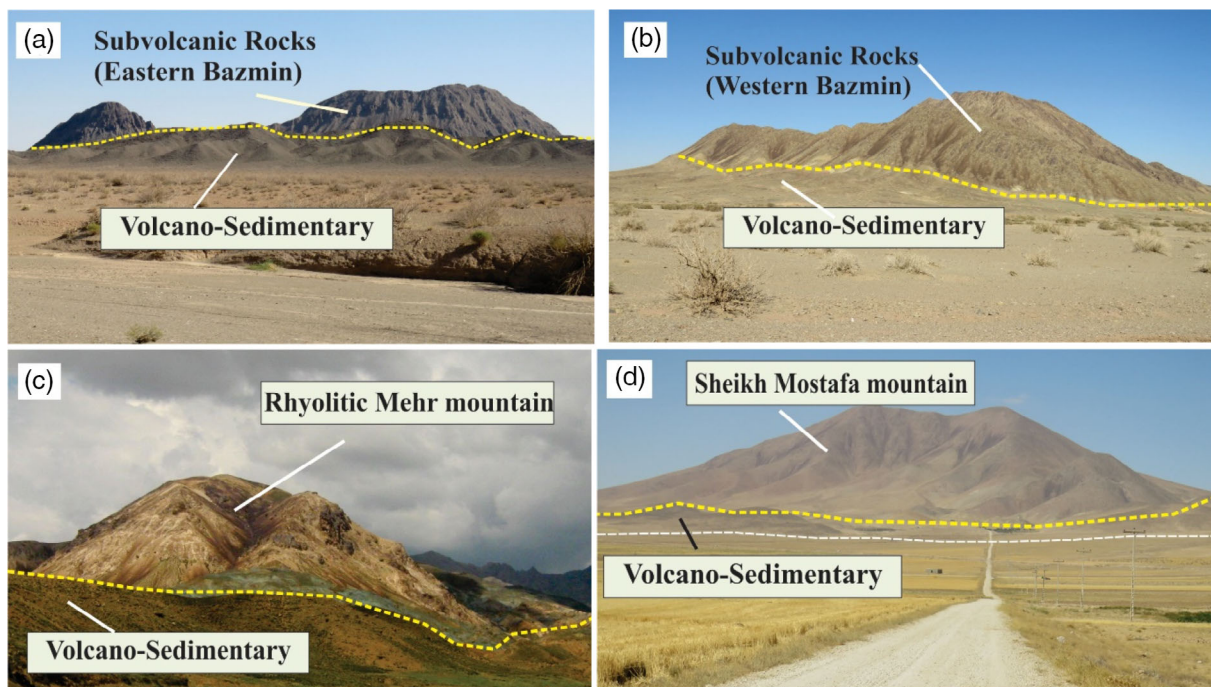

FIGURE 2 Field photographs of hypabyssal intrusive rocks in the studied areas. (a and b) Bazmin (left) and east of Bazmin (right) and felsitic and dacitic mountains in south and southeast Shahrood. (c and d) Field photograph of rhyolitic Mehr in Sabzevar region (left) and Sheikh Mostafa (right) domes in Qouchan-Esfarayen magmatic belt [Colour figure can be viewed at wileyonlinelibrary.com]

Iranian microcontinent that then collides with the Eurasian Plate (Shahabpour, 2007). From the Late Carboniferous, rifting occurred and the Neo-Tethys Ocean began opening (Berberian & Berberian, 1981). Movement to the north of the Arabic Plate during the Triassic-Jurassic leads to the subduction of the Neo-Tethys oceanic plate beneath the Central Iran Plate (Stampfli & Borel, 2002). Berberian and Berberian (1981), Guest, Horton, Axen, Hassanzadeh, and McIntosh (2007), and Allen and Armstrong (2008) suggest that the last time the Neo-Tethys Ocean closed and the collision between the Arabian Plate and Central Iran occurred was during the Neogene. The subduction of the Neo-Tethys oceanic lithosphere under the southwestern part of Central Iran led to the development of intrusive and coeval volcanic activity between the Jurassic and Quaternary, as well as the southern margin of Central Iran (Mohajjel, Fergusson, & Sahandi, 2003). The Sanandaj Sirjan Zone (SSZ), CISZ, and UDMA can be considered as a segment of the upper plateau (Eurasia) during the convergence and collision of the Arab-Eurasian Plate.

The collision of two continental plates produced tectonic and magmatic features, such as the Urmia-Dokhtar magmatic arc (UDMA); many of these Zagros tectonic structures have been recorded throughout Cenozoic (Stocklin, 1968) and the UDMA represent a central segment of the broader Alpine–Himalayan belt that extends from western Europe to eastern Pakistan. Omrani et al. (2008) noted that the Zagros Mountains are part of the Alpine–Himalayan orogenic belt and resulted from the closure of the Neotethyan ocean between Arabia and Eurasia. Many scientists have referred to the Zagros orogeny and magmatic activity affected by it, such as Aftabi and Atapour (2009). The closure of the Neo-Tethys Ocean lead to the collision between the African and Eurasian plates leading to the formation of the continental volcanic arc during the Tertiary (Fu, McInnes, Evans, & Davies, 2010; Sengor & Kidd, 1979; Shafiei, Haschke, & Shahabpour, 2009). The magmatism in the UDMA originated in the early Eocene and peaked in the Middle Eocene (Berberian & King, 1981).

The tectonic position of the three regions mentioned above is described as follows: Qouchan-Esfarayen magmatism is located in the 60 km south of Qouchan and 50 km east of Esfarayen. Qouchan-Esfarayen magmatism extended from the northwest to the southeast and is situated between longitudes 57° 18′ to 58° 47′ East and latitude 36° 37′ to 36° 58′ North (Gardideh et al., 2018). Adakitic rocks intruded into the Sabzevar ophiolite that is situated in the Sabzevar metamorphic and ophiolitic zone with an overall length of 200 km and approximate width 10 km and located between longitudes 56° 26′ and 57° 33′ East and latitude 36° 22′ and 36° 35′ North. This large
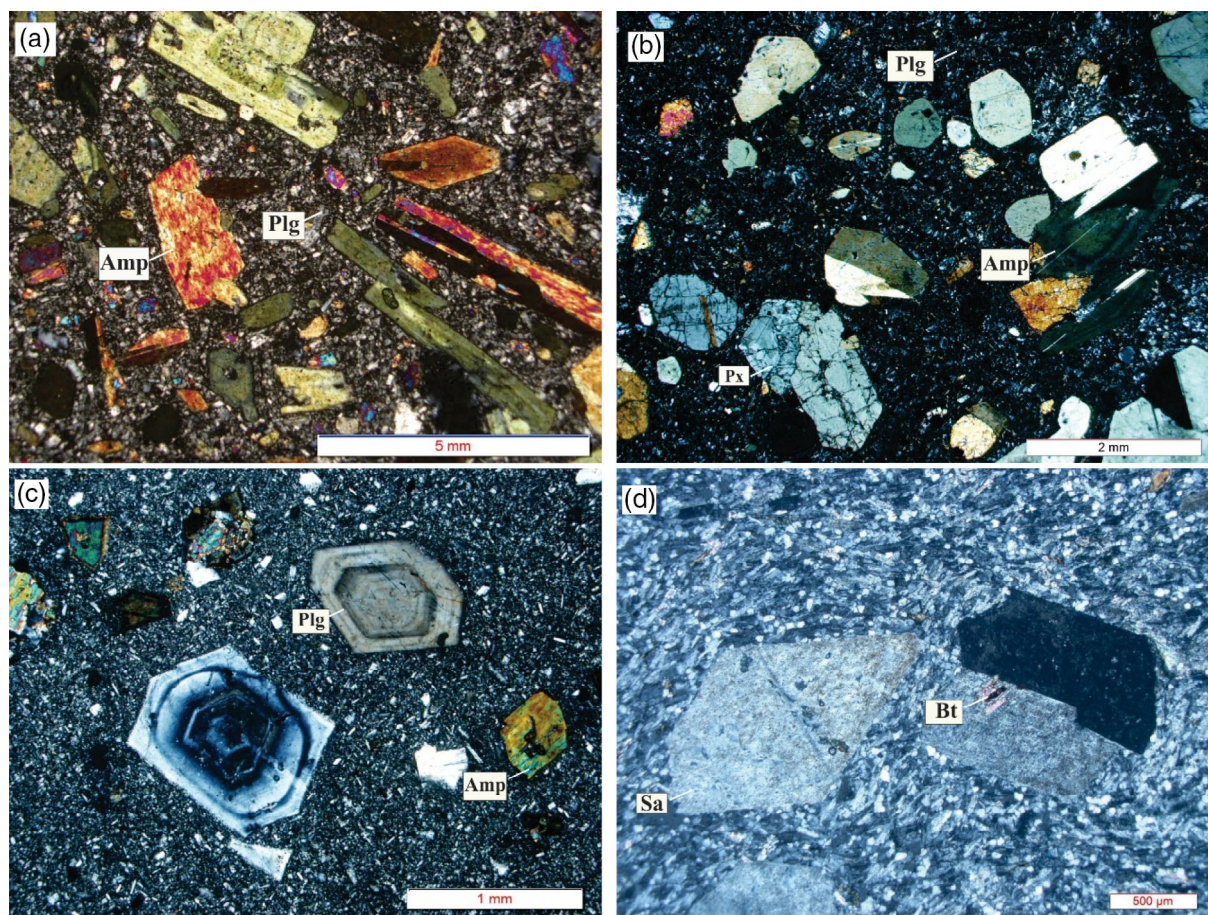

FIGURE 3 Photomicrographs (cross-polarized transmitted light) of studied samples. (a) Abundant amphibole (Amp) and plagioclase (Plg) phenocrysts in trachyandesite. (b) Pyroxene (Px), amphibole, and plagioclase phenocrysts in microcrystalline basaltic andesite. (c) Microcrystalline dacite with oscillatory zoned plagioclase phenocrysts. (d) Plagioclase, sanidine (Sa), and biotite (Bt) phenocrysts in a microcrystalline rhyolite. (Abbreviations for rock-forming minerals from Whitney & Evans, 2010) [Colour figure can be viewed at wileyonlinelibrary.com]

ophiolite complex is located along the northern CISZ (Jamshidi et al., 2018). Adakite magmatism is situated 120–160 km south-southeast of Shahrood and Damghan (east of Semnan Province, NE Iran), in the northern part of the CISZ and are between longitudes 55° 20′ to 56° 10′ East and latitude 35° 40′ to 36° 00′ North (Yousefi, Sadeghian, Samyari, & Ghasemi, 2017) (Figure 2). The oldest rock units in this region are the Late Neoproterozoic units (Balaghi Einalou, Sadeghian, Minggou, Ghasemi, & Mohajjel, 2014; Hosseini, Sadeghian, Minggou, & Ghasemi, 2015), which include mica schist, metapsammite, metacarbonate, paragneiss, amphibolite, and mylonitized granites.

2.2 | Rock types and Petrography

Based on the U–Pb zircon dating, the age of the rocks of south-southeast Shahrood, which is famous within the Torud-Ahmad Abad magmatic belt, lies between 41.4 ± 0.3 Ma and 35.5 ± 0.2 Ma (Yousefi, Sadeghian, Samyari, & Ghasemi, 2017), with the age of adakite rocks emplaced into the Sabzevar ophiolite at about 45 Ma (Jamshidi et al., 2015). However, the age of the igneous rocks in Qouchan-Esfarayen magmatic belt is younger yielding 17.83 ± 0.24 Ma and 8.50 ± 0.34 Ma (Gardideh et al., 2018). These differences in age are due to certain tectonic events that will be discussed further. The age range of these rocks extends from Middle Eocene to Late Miocene. According to petrographic studies, the hypabyssal rocks in these magmatic belts have a wide range of compositions from trachybasaltic andesite, andesite, trachyandesite, dacite, trachyte to rhyolite. Felsic rocks of dacite to rhyolite composition crop out as dominantly light grey to white-coloured domes in the southern and southwestern part of the Sabzevar belt. Dacite rocks in these regions (adakitic magmas were emplaced into the Sabzevar ophiolite, igneous rocks in Qouchan-Esfarayen magmatic belt, and the adakitic rocks of south-southeast Shahrood) have a grey to light grey appearance and their main phenocrysts are amphibole and plagioclase that locally have a trachytic texture. Some amphiboles are completely black in a microcrystalline grey groundmass. The black colour of these amphiboles is thought to be due to the oxidation of these minerals during magma ascent. In the hand specimen, the rhyolites are pinkish-white to cream colour with glassy to aphanitic with a locally porphyritic texture. Rhyolite samples show quartz (embayed to rounded quartz), sanidine (altered sanidine), and plagioclase phenocrysts within a very fine-grained (microcrystalline) groundmass (Figure 3).

In some rocks of the Sabzevar region, the amphiboles from the andesitic samples are Mg-hastingsites to tschermakites, those in the trachyandesite and trachydacite samples are tschermakite, and those amphiboles from dacites are mostly magnesiohornblende (Jamshidi et al., 2015). The composition of plagioclase phenocrysts in the andesite and trachyandesite rocks range from $An_{53}Ab_{46}Or_1$ to $An_{70}Ab_{29}Or_1$ and $An_{36}Ab_{62}Or_2$ to $An_{56}Ab_{43}Or_1$, respectively. Plagioclase is the volumetrically dominant phenocryst phase in the trachydacite ($An_{31}Ab_{67}Or_2$ to $An_{49}Ab_{51}Or_1$) and dacite ($An_{40}Ab_{58}Or_2$ to $An_{24}Ab_{73}Or_3$) samples, but is rare in the rhyolites ($An_{15}Ab_{80}Or_5$ to $An_8Ab_{88}Or_4$). Pyroxenes are in the range of diopside to augite (Jamshidi et al., 2015). Andesitic and basaltic andesite are grey to grey-green and occur widely in the Torud-Ahmad Abad magmatic belt. Major constituent minerals of andesite and basaltic andesite rocks include amphibole, plagioclase, and pyroxene (Figure 3b). According to Yousefi, Sadeghian, Wanhainen, et al. (2017), the plagioclase are mainly albite, andesine, and labradorite, amphiboles are in the range of pargasite to magnesian-hastingsite, and clinopyroxene have a diopside composition with some in the augite range. In all rock groups, apatite and biotite are common accessory minerals. Calcite, sericite, chlorite, epidote, and iron oxides are secondary alteration minerals. These rocks contain the porphyritic, granular, glomeroporphyritic, trachytic, and sieved textures in some plagioclase. An interesting feature, especially within andesite and dacite, is the presence of zoning in plagioclase and some amphibole phenocrysts. Normal zoning in plagioclase shows a compositional change from calcic (cores) to less calcic with progressive growth. According to Blundy and Shimizu (1991) and Yousefi, Sadeghian, Wanhainen, et al. (2017), zoning in minerals record both the chemical and physical changes to the evolving magmatic liquids. The rapid and local changes of molten compounds cause the formation of the observed complex zoning phenomenon (cf. Vernon, 2008).

3 | ANALYTICAL METHODS

Least-altered samples (n = 66) were selected for whole-rock geochemical (lithogeochemistry) and petrographic analysis. All samples represent extremely rare examples of unaltered (fresh) to least-altered varieties and generally undeformed igneous rocks. The samples were analysed for major and selected trace elements by fusion inductively coupled plasma-emission spectroscopy (ICP-ES) after fusion of 0.2 g of rock powder with 1.5 g $LiBO_2$ and dissolved in 100 mL 5% HNO_3. Rare-earth element (REE) analyses were performed by fusion inductively coupled plasma-mass spectroscopy (ICP–MS) at ACME and ALS Chemex Company in Canada. Detection limits range 0.01–0.1 wt% for major oxides, 0.1–10 ppm for trace elements, and 0.01–0.5 ppm for REEs. Loss on ignition was determined by heating the samples at 1,000°C.

Eleven samples with nominal prefix FY and FR were isotopically analysed on the basis of estimated or previously determined element concentrations. Strontium was purified using Sr-spec cation exchange resin using the methods of Lundblad (1995) and loaded on single Re filaments with a TaF_5 activator to enhance ionization. Neodymium was purified through a three-stage column chemistry procedure following Harvey and Baxter (2009). Total procedural blanks were less than 0.1 ng for Sr and 0.02 ng for Nd. Whole-rock Nd and Sr isotopes were analysed on the Isotopix Phoenix X62 TIMS at the University of North Carolina at Chapel Hill. Strontium was analysed as a metal in dynamic multicollector mode with ^{88}Sr = 3 V. Strontium isotope ratios were corrected for mass fractionation using an exponential law correction and normalized to $^{86}Sr/^{88}Sr$ = 0.1194. Replicate analyses of the NBS 987 Sr standard yielded $^{87}Sr/^{86}Sr$ = 0.710243 ± 11 (2σ, n = 10). Neodymium was analysed in dynamic-multicollector mode with ^{147}Sm = 3 V, $^{142}Nd^{16}O$ = 1 V (Yousefi, Sadeghian, Samyari, &

Ghasemi, 2017). The remaining samples have been analysed at Institute of Geology and Geophysics, Chinese Academy of Sciences (IGG-CAS). These analytical procedures are explained in detail in Jamshidi et al. (2018) and Gardideh et al. (2018).

4 | WHOLE-ROCK GEOCHEMICAL RESULTS

4.1 | Major and trace elements

The results of whole geochemical analysis are presented in supplementary Table 1 s, 2 s, and 3 s. In this supplementary document, geochemical data of hypabyssal rocks from south to southeast Shahrood, Sabzevar, and Qouchan areas are presented. Other related information are presented in Jamshidi et al. (2018) and Rezaei Kahkhaei, Taheri Sarteshnizi, Ghasemi, and Gardideh (2018).

The compiled samples in Table 1s, 2 s, and 3 s contain SiO_2 of 51.06–73.62 wt% (see Figures 4 to 11). Their Na_2O and K_2O contents range from 2.73 to 6.97 wt% and from 0.59 to 3.75 wt%, respectively, with K_2O/Na_2O ratios of 0.14–1.0. The amount of Al_2O_3 is between 14.25 and 19.07 wt%. According to Le Bas, Le Maitre, Streckeisen, and Zanettin (1986), the studied rocks plot in the range of basaltic andesite, andesite, trachyandesite, dacite, trachyte, and rhyolite (Figure 4a). Based on diagram A/NK (molar $Al_2O_3/[Na_2O + K_2O]$) vs. A/CNK (molar $Al_2O_3/[CaO + Na_2O + K_2O]$) (Figure 4b), the samples show metaluminous and peraluminous signatures, and the diagram of Peccerillo and Taylor (1976), these samples plot in the field of normal calc-alkaline and high-K calc-alkaline suites (Figure 4c). Mg# [100*MgO/(MgO + FeO)] ranges from 33.8 to 82.4 (Figure 4d).

Most major oxide and trace element variations display negative or positive correlations with increasing SiO_2 relative to their compatibility. There is a decrease for FeO total, TiO_2, MnO, MgO, and Zr/Nb vs. SiO_2, whereas an increase for Na_2O, K_2O, La/Yb, and Rb/Sr (Figure 5). These samples show LREE enrichment and HREE depletion in chondrite-normalized REE patterns (Figure 6). Strong enrichments in large-ion lithophile elements (LILE) are obvious, such as Rb, Ba, Th, and U and depletion in compatible HFSE, such as Nb, Ta, and Ti. According to Mahmoudi Nia, Baghban, and Simmonds (2017), high Sr content and the negative anomalies of Ti, Ta, and Nb shows a lack of plagioclase fractionation and occurrence of Fe and Ti oxides throughout partial melting and crystal fractionation. Richards, Spell, Rameh, Razique, and Fletcher (2012) thought that depleted MREE-HREE strongly propose REE fractionation controlled by hornblende leading to low Y and Yb (HREE) concentrations decreasing with increasing SiO_2.

In some rhyolitic samples, there are a few negative Eu anomalies. Partitioning of Eu^{+2} between plagioclase and melt is affected by oxygen activity. Eu^{+2} dominates at low oxygen activities and Eu^{+3} at high oxygen activities (cf. Drake & Weill, 1975; Rollinson, 1993). Eu^{+2} is more compatible than Eu^{+3} in plagioclase. At high oxygen activities, partition coefficients for Eu are very low (into feldspar) like the other trivalent REE, although at low oxygen activities this is opposite (Rollinson, 1993). Therefore, crustal interactions may have affected the redox behaviour of the more evolved felsic magmas due to minimal buffering capacity, leading to variable Eu anomalies. According to Han et al. (1997), negative Eu anomalies in some rhyolitic samples reflect plagioclase fractionation. Also, Azer (2007) documented that differential fractionation of a small amount of plagioclase or partial melting that leaves plagioclase in the source can lead to such abnormalities (variable δE) in the remaining (derivative) melt.

4.2 | Sr and Nd isotopes

Whole-rock Sr and Nd isotopic compositions are presented in Table 1 and supplementary Tables 4s and 5 s. Initial Sr and Nd isotope ratios and epsilon values (εNd) of these adakite rocks were calculated using ages of 41.4 ± 0.3 Ma and 35.5 ± 0.2 Ma in south to southeast Shahrood, 45 Ma for adakite magmatism within the Sabzevar ophiolite, and 17.83 ± 0.24 Ma, and 8.50 ± 0.34 Ma for Qouchan-Esfarayen magmatism. The adakitic rocks in Qouchan-Esfarayen magmatism have 0.512581 to 0.51288 initial $^{143}Nd/^{144}Nd$ and 0.703903 to 0.705627 initial $^{87}Sr/^{86}Sr$ and εNd −0.86 to 4.98. South to southeast Shahrood has 0.512775 to 0.512893 initial $^{143}Nd/^{144}Nd$ and 0.703746 to 0.705314 initial $^{87}Sr/^{88}Sr$ with εNd 3.69 to 6.00. Adakite rocks emplaced into the Sabzevar ophiolite have 0.512846 to 0.512911 initial $^{143}Nd/^{144}Nd$ and 0.70379 to 0.705019 initial $^{87}Sr/^{86}Sr$ contents with εNd of 5.26 to 6.54.

5 | DISCUSSION

In this section, we focus on magma petrogenesis, magmatic evolution, and source characteristic debates, exploring geodynamic implications and then also provide further subtle details in these adakitic suites.

5.1 | Magma petrogenesis

Geochemical characteristics, such as SiO_2 of 51.06–73.62 wt%, Al_2O_3 = 14.25–19.07 wt%, Sr = 138–1,219 ppm, Yb = 0.10–2.12 ppm, and Y = 2.7–18 ppm contents, with high Sr/Y = 7.30–279, and $(La/Yb)_N$ = 1.43–30.9 ratios, show distinct adakite and adakite-like signatures (Figure 7). These samples generally plot in the adakitic field on Sr/Y vs. Y diagram (Defant & Drummond, 1990). All the samples contain high concentrations of Sr and low concentrations of Y and Yb (ppm) contents similar to those in the range observed in typical adakites. According to Chen et al. (2016), the chemical differences between LSAs (solid field) and HSAs indicate the effects of garnet (Grt), amphibole (Am), zircon (Zrn), and apatite (Ap) fractionation on Sr/Y and Y (Yb) on adakites. Ma, Zheng, Xu, Griffin, and Zhang (2015) suggested that the term adakite be limited to defining intermediate-felsic igneous rocks resulting from melting of subducted oceanic slabs.
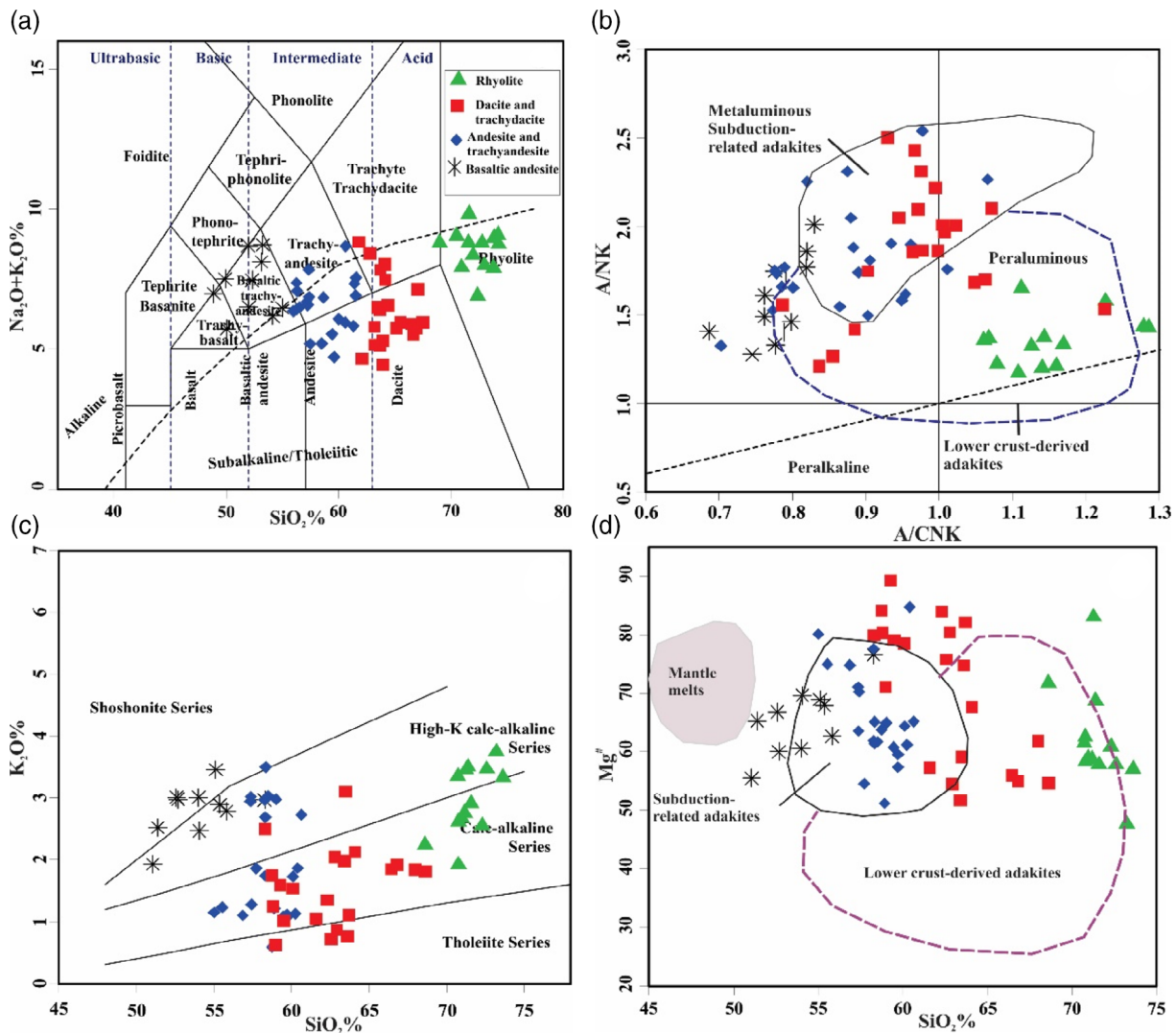
FIGURE 4 (a) Compositions of rocks in the northern part of the Central Iran Structural Zone. (b) A/CNK vs. A/NK diagram from Maniar and Piccoli (1989). (c) K₂O vs. SiO₂ diagram of Peccerillo and Taylor (1976), the samples plot in the fields of calc-alkaline and high-K calc-alkaline. (d) SiO₂ vs. Mg # diagram from Guan et al. (2010). All symbols are the same in all figures [Colour figure can be viewed at wileyonlinelibrary.com]

According to Nakamura and Iwamori (2013), adakite rocks may also be derived from melting of the mantle metasomatized by fluids released during dehydration of subducting oceanic lithosphere, with other components coming from the overlying lithosphere (subcrustal–suprasubduction zone) and (or) subducted sediments. The various evidence of arc magmatism are enrichment of LILE and LREE and depletion in HFSE and HREE, relative negative anomalies in Nb, Ta, Hf, Zr, and Ti, and presence of hydrous minerals, such as biotite and amphibole (Eyuboglu, Santosh, & Chung, 2011; Ringwood, 1990). This geochemical evidence reflects an arc-related subduction environment (Deng et al., 2017; Murphy, 2007). According to the Al_2O_3 vs. TiO_2 diagram, these samples fall within the arc-related field (Figure 8a). Also by comparing the ratio of Nb/Yb vs. Th/Yb, the samples plot along the volcanic arc array (Figure 8b). Detailed results of these areas have been presented separately (Gardideh et al., 2018; Jamshidi et al., 2018; Yousefi, Sadeghian, Samyari, & Ghasemi, 2017; Yousefi, Sadeghian, Wanhainen, et al., 2017). According to Maruyama (1997) on the changes

in magnesium number, we note that the melt that reacts with mantle peridotite creates low-SiO₂ adakites. During rapid ascent, there may be interactions between the felsic melts and peridotite increases the Mg-number, while the amount of SiO_2 is also slightly reduced (Eyuboglu, Chung, Santosh, Dudas, & Akaryal, 2011). Rapp, Shimizu, Norman, and Applegate (1999) explained that if the interaction between the felsic and mafic melts is more than 15%, magnesium number (Mg#) increases as SiO₂ decreases.

Chiaradia (2015) has pointed out the ratio of Sr/Y in the magmas of arc environment is high, which is similar to these studied igneous rocks where the ratios of Sr/Y and La/Yb are high. Chiaradia (2015) also noted that crustal thickness has a significant control on Sr/Y variability of arc magmas through the stabilization or destabilization of mineral phases that fractionate Sr (plagioclase) and Y (amphibole and garnet). High ratios of Sr/Y (>20) indicate a lack of plagioclase fractionation combined with the existence of garnet in the source and it is evidence of partial melting of an eclogitic source (Richards et al., 2012). Based on Castillo (2008) and
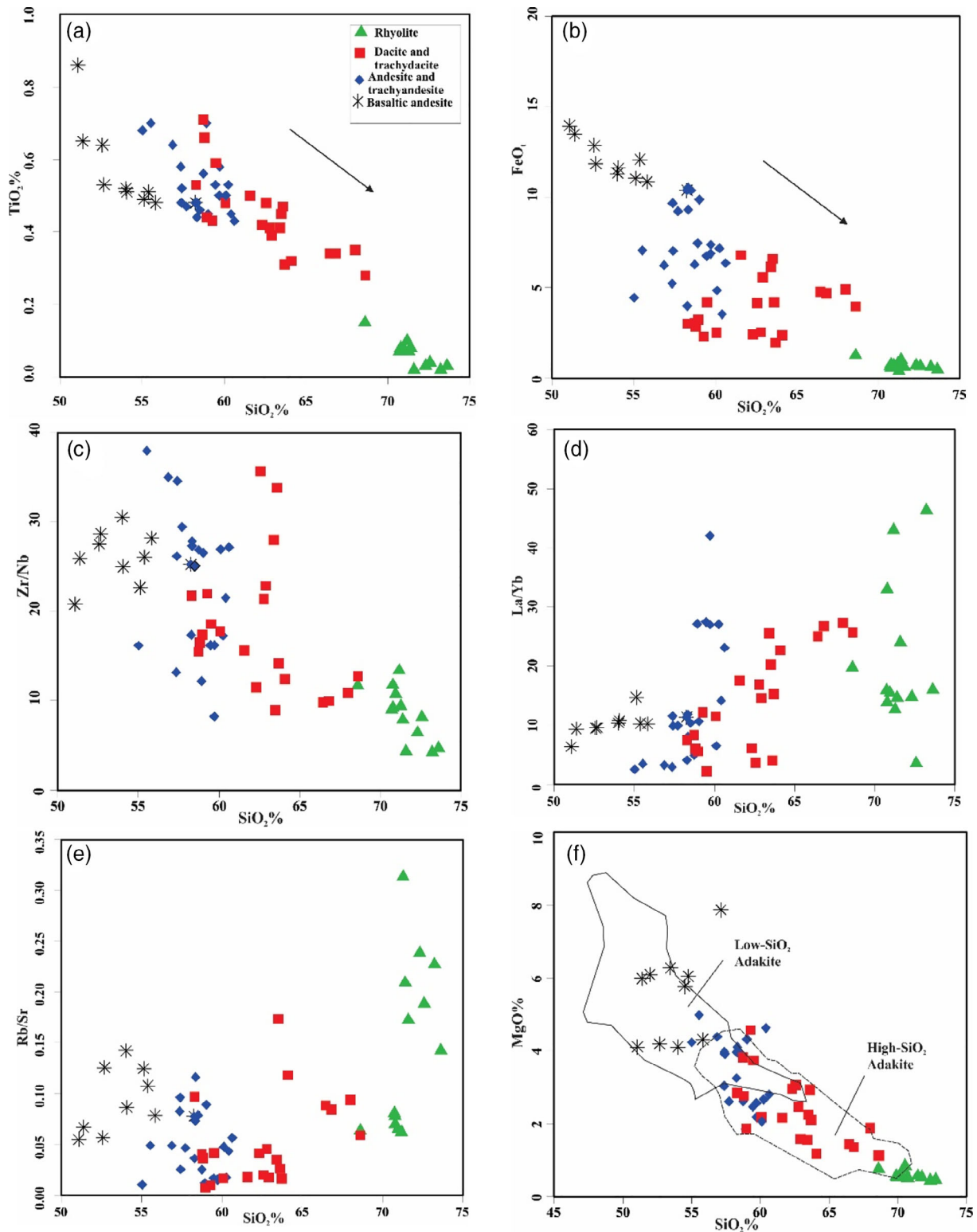
FIGURE 5 Harker (1909) diagrams of key elements and element ratios illustrating the distribution of the data. All symbols are as in Figure 3. The process marked with the arrow in Figure 5a,b reflect the significant role of fractional crystallization processes of different mineral phases during the evolution of the volcanic suites. In Figure 5f, we classified the low-silica adakites (LSA) and high-silica adakites (HSA) (modified from Castillo, 2012) [Colour figure can be viewed at wileyonlinelibrary.com]

Richards and Kerrich (2007), high contents of Ba and Sr and no significant Eu anomalies, with depleted HREE and Y patterns, show garnet residue and the absence of plagioclase in their source region (Figure 6). With a

comparison between the adakitic rocks in these regions and the adakitic rocks in eastern China (Wang, Zhang, Liu, & Que, 2016), the high proportion of the elements, such as K, Ba, Rb, and Sr, suggests that the parental
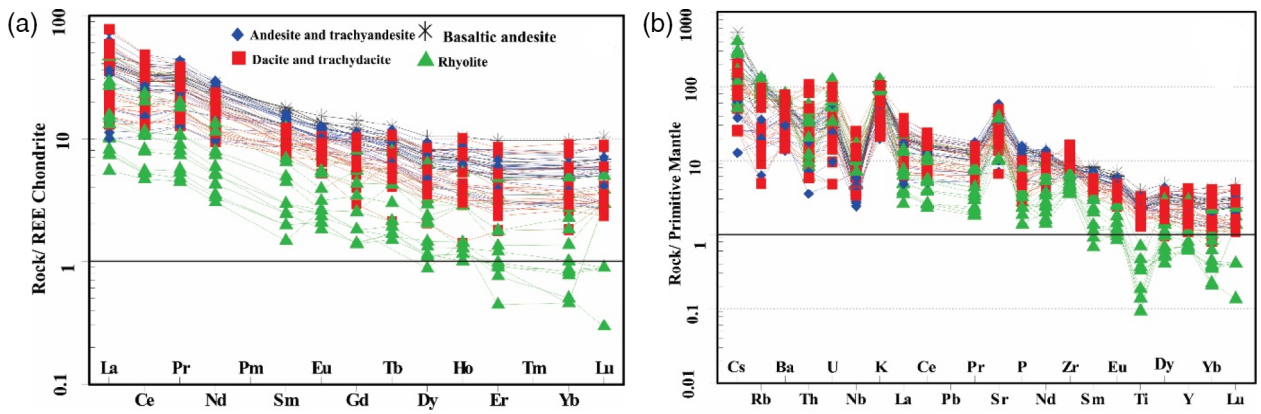
FIGURE 6 (a) Chondrite-normalized REE pattern (Nakamura, 1974). (b) Primitive mantle-normalized trace element variation diagrams (Sun & McDonough, 1989). All symbols are as in Figure 3 [Colour figure can be viewed at wileyonlinelibrary.com]
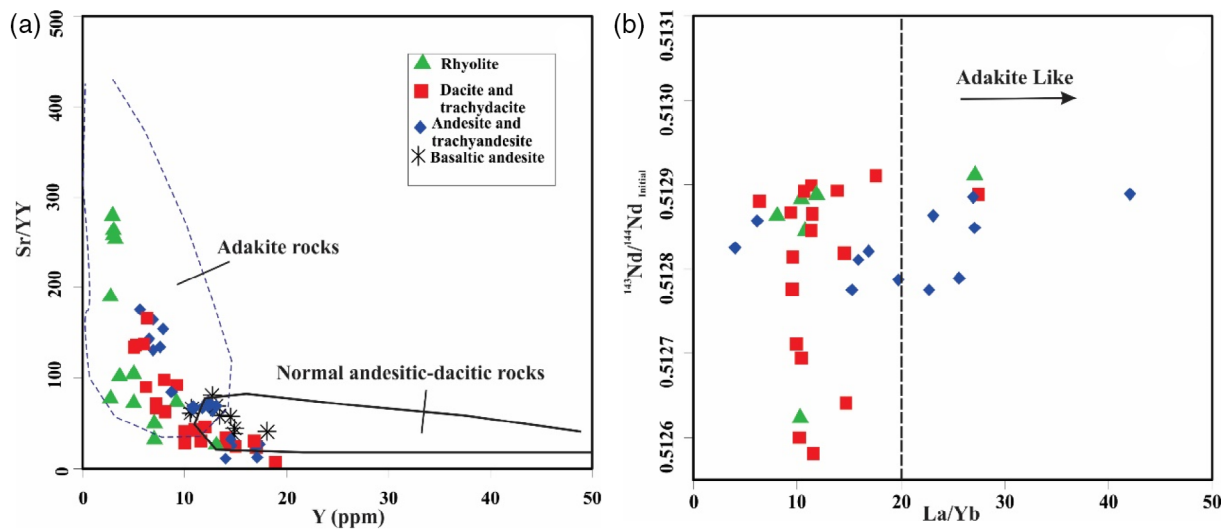

FIGURE 7 (a) Sr/Y vs. Y discrimination diagram (Defant & Drummond, 1990). (b) $^{143}Nd/^{144}Ndi$ vs. La/Yb (Kolb et al., 2013) [Colour figure can be viewed at wileyonlinelibrary.com]
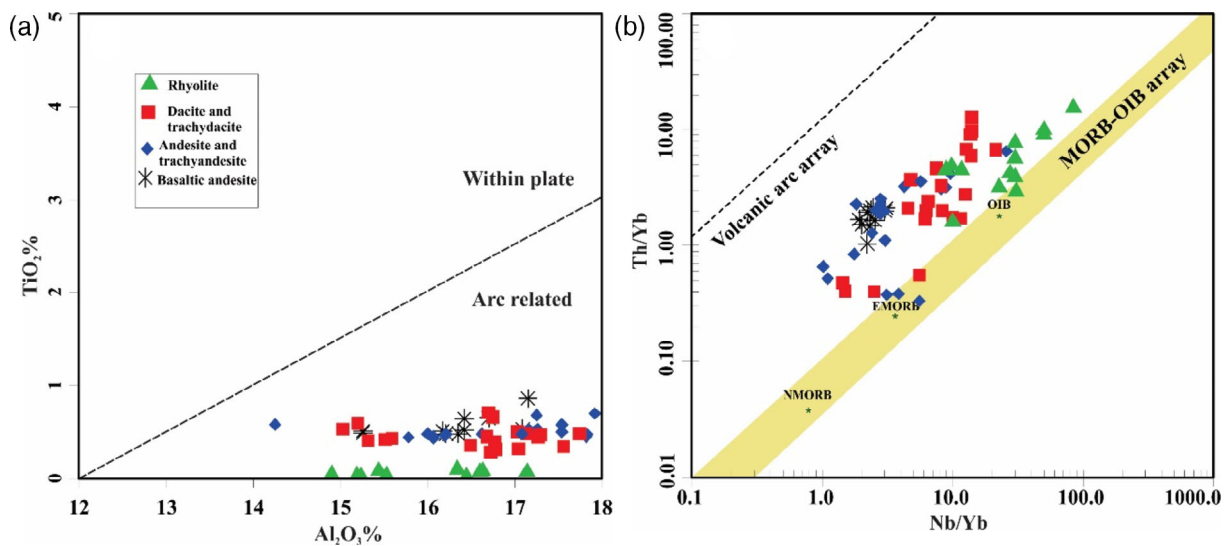

FIGURE 8 Tectonic discrimination diagrams for adakitic rocks in the CISZ. (a) Al_2O_3 vs. TiO_2 diagram from Müller and Groves (1993). (b) Nb/Yb vs. Th/Yb diagram from Pearce (2014) [Colour figure can be viewed at wileyonlinelibrary.com]
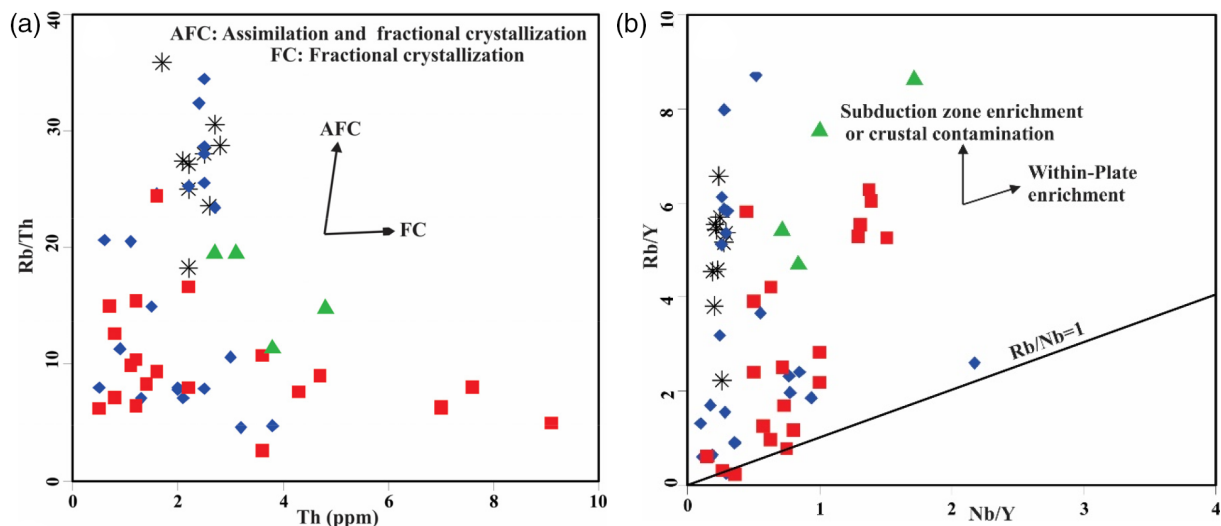
FIGURE 9 (a) Th vs. Rb/Th diagram to distinguish the processes of assimilation and fractional crystallization or fractional crystallization in the development of these rocks (Pearce, 1983). (b) Nb/Y vs. Rb/Y diagram (Pearce, 1983) [Colour figure can be viewed at wileyonlinelibrary.com]

magmas are most likely derived from partial melting of the subducted oceanic crust. Similar conditions of these areas have been introduced by Temizel, Arslan, Yücel, Abdioğlu, and Ruffet (2016). They believe that the Pontides of northern Turkey were formed as a consequence of northward subduction of the Neo-Tethys Ocean along the Eurasian margin. This area has similar geochemical characteristics to the studied areas. Based on a recent analysis on the melt inclusions that were hosted within plagioclase phenocrysts in andesite, trachyandesite, basaltic andesite, and dacite, it was found that the crystallized melt inclusions in these rocks exhibited considerable intrasample diversity that relates to petrogenesis and compositional evolution (Yousefi, Papadopoulou, Sadeghian, Wanhainen, & Bark, 2019).

5.1.1 | Magmatic evolution

Macpherson, Dreher, and Thirlwall (2006) determined that a high ratio of Sr/Y is due to assimilation and fractional crystallization (AFC) processes of mantle-derived magmas, whereas Defant and Drummond (1990), Rapp et al. (1999), and Deng et al. (2017) proposed partial melting of subducted oceanic slabs. Based on Harker diagrams (Figure 5), the role of selective partial melting, followed by variable fractional crystallization (FC) is quite evident. In Figure 5f, the adakitic rocks classified as HSA and LSA (see Castillo, 2012). Usually the amount of TiO_2, MgO, CaO, FeO_t, Y, Ce, and Nd in intermediate and felsic rocks has the lowest concentration and the amount of K_2O and Al_2O_3 does not have a systematic trend. Eyuboglu, Santosh, and Chung (2011) suggested that this downward trend is due to low-pressure FC of minerals, such as clinopyroxene, Fe–Ti oxides, biotite, and apatite crystallized during evolution of adakitic magmas, with systematic trends due to the alteration of some minerals, such as plagioclase and K-feldspar. Decrease in P_2O_5, TiO_2, and Sr content corresponds to an increase in SiO_2 content that is probably related to apatite, Fe-Ti oxide, and plagioclase fractionation. Temizel, Arslan, Ruffet, and Peucat (2012) and
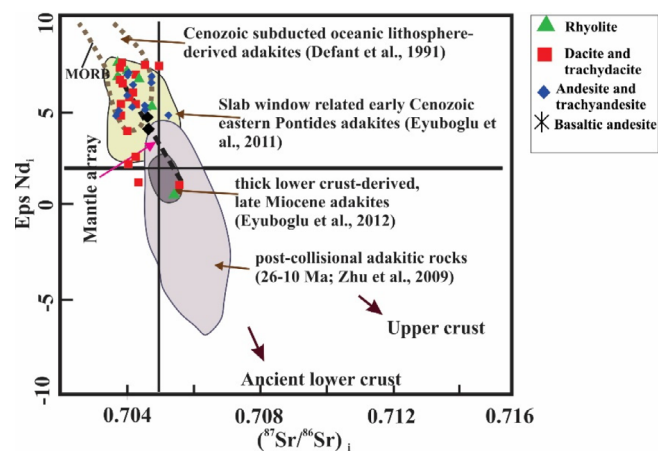

FIGURE 10 $^{87}Sr/^{86}Sr$ (i) vs. $\varepsilon Nd(i)$ diagram of the studied rocks plotting in the Cenozoic subducted oceanic lithosphere derived adakite field (cf. Defant et al., 1991) [Colour figure can be viewed at wileyonlinelibrary.com]

Temizel (2014) believed that these correlations and decreases of CaO with increasing SiO_2 reflect the significant role of FC processes of different mineral phases, such as clinopyroxene and plagioclase during the evolution of the volcanic suites.

Rollinson (1993) observed that systematic changes in trace elements typically reflect petrological processes. In this part, we use the Th vs. Rb/Th diagram (Pearce, 1983) to assess the role of assimilation with FC (AFC) and FC during the evolution of these magmatic rocks. The Nb/Y vs. Rb/Y diagram and Th changes show the magmas forming these rocks have undergone minor crustal contamination (Figure 9). According to studies done by Lucci et al. (2016) on part of calc-alkaline magmatic rocks in Sabzevar region, hornblende is the main phase that controls REE and Y differentiation and fractionation. They also emphasize the role of the Tschermak molecule ($CaAlAlSiO_6$) in the fractionating hornblende and plagioclase assemblage during arc-like magma differentiation.
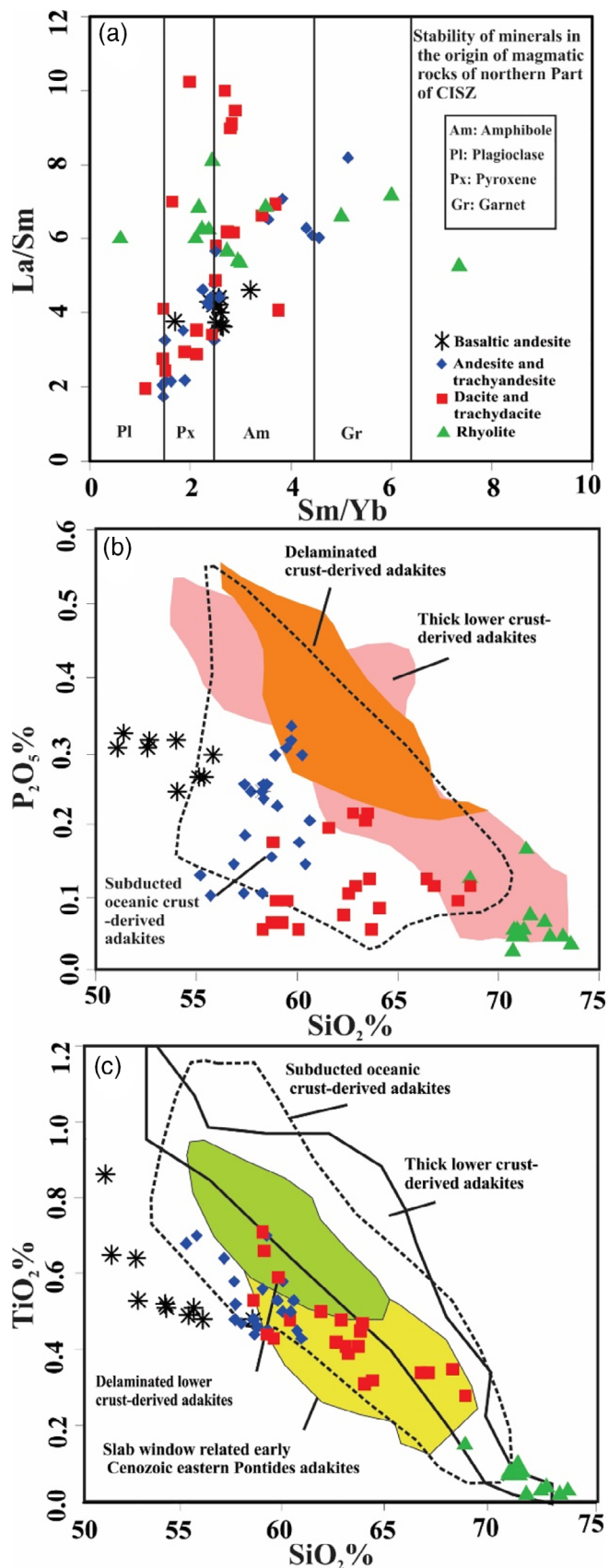
In these rocks, there are numerous enclaves with variable compositions, such as mafic microgranular enclaves, mafic clot (rich in hornblende and a little pyroxene), mica schist, biotite gneiss, amphibolite, leucogabbro, marl, tuffaceous shale, and sandstone, which are visual signs of magma mixing and crustal contamination (Jamshidi et al., 2015; Yousefi, Sadeghian, Samyari, & Ghasemi, ; Yousefi, Sadeghian, Wanhainen, et al., 2017). Rollinson (1993) and John, Klemd, Klemme, Elis Hoffmann, and Gao (2011) pointed out that a negative anomaly of Nb and Ta and increase of Rb, Ba, and K show the role of magma mixing between basic magma and adakite magma and crustal contamination in the evolution of these magmatic rocks.

5.1.2 | Source characteristics

To determine the origin of the studied rocks in the three areas mentioned, the $\varepsilon Nd(i)$ vs. $^{87}Sr/^{86}Sr(i)$ diagram has been used (Figure 10). The Cenozoic magmatism in south and southeast Shahrood (Torud-Ahmad Abad magmatic belt), Sabzevar, and Qouchan-Esfarayen plot in the field outlined for Cenozoic subducted oceanic lithosphere-derived adakites (Figure 10). In these adakitic and adakite-like rocks, $\varepsilon Nd(i)$ values are high and $^{87}Sr/^{86}Sr$ ratios are quite low (details of these ranges are presented in Defant et al., 1991; Eyuboglu, Santosh, & Chung, 2011; Eyuboglu, Santosh, Yi, Bektaş, & Kwon, 2012; Zhu et al., 2009). Kay (1978) thought that adakitic rocks were related to convergent plate margin arcs through melting of oceanic crust. Mahmoudi Nia et al. (2017) pointed out that in NW Iran, there are some adakitic rocks that are related to subduction of Neo-Tethyan oceanic lithosphere.

As shown in Figure 10, most samples are in the range of Cenozoic subducted oceanic lithosphere-derived adakites. For some of the samples that belong to Qouchan-Esfarayen region, the ratios of $^{87}Sr/^{86}Sr$ are high and $^{143}Nd/^{144}Nd$ are low. According to petrographic evidence and geochemical signatures and the magma separation process yield rocks from trachyandesite to rhyolite; along with field and chemical evidence, this evidence shows that these rocks have the same origin as other groups. However, they exhibit contamination with continental crust possibly during ascent. Therefore, it can be said that these hypabyssal rocks in the Qouchan-Esfarayen magmatic belt originated from melting of the subducted metamorphosed Neo-Tethys oceanic slab (Sabzevar branch) that was contaminated with continental crust during emplacement. Stern and Scholl (2010) noted that continental crust is created and destroyed by plate tectonic processes formed by arc magmatism and eliminated by subduction. The

FIGURE 11 (a) Sm/Yb vs. La/Sm to determine the stability of minerals in the source region where melts form (see Haschke & Ben-Avraham, 2005). (b and c) P_2O_5 and TiO_2 vs. SiO_2 diagrams with various compositional (outlined) fields from Wang et al. (2004, 2006) [Colour figure can be viewed at wileyonlinelibrary.com]

FIGURE 11 Legend on next page.

TABLE 1 Nd and Sr isotopic data from samples of rocks in south-south east of Shahrood

Sample	Nd (ppm)	Sm(ppm)	$^{143}Nd/^{144}Nd$ m	$^{143}Nd/^{144}Nd$ i	εNd	Sr (ppm)	Rb (ppm)	$(^{87}Sr/^{86}Sr)$ m	$(^{87}Sr/^{86}Sr)$ i
FY-2-2	21.80	3.45	0.512845	0.512819	4.57	1,080	20.00	0.703917	0.703886
FR-6	16.50	3.58	0.512824	0.512789	3.97	591	28.50	0.704701	0.704620
FY-7a	15.40	2.99	0.512896	0.512865	5.45	926	15.30	0.703896	0.703868
FR-26	13.40	3.23	0.512896	0.512857	5.30	548	66.30	0.704998	0.704794
FR-32	13.40	3.24	0.512814	0.512775	3.70	850	49.40	0.705412	0.705314
FR20	13.90	3.10	0.512857	0.512821	4.60	864	68.40	0.704732	0.704599
FR22	23.30	3.67	0.512813	0.512787	3.94	1,041	22.30	0.703869	0.703833
FR28	12.80	2.85	0.512861	0.512825	4.67	837	54.20	0.704188	0.704079
FY33	11.20	2.11	0.512805	0.512775	3.69	796	17.70	0.703784	0.703746
FR63	11.60	2.42	0.512845	0.512811	4.41	912	65.00	0.704347	0.704227
FY7b	16.70	3.00	0.512922	0.512893	6.00	896	16.70	0.703885	0.703854

geochemical properties of these three neighbouring regions including depletion of HREE plus high ratio Sr/Y and $(Gd/Yb)_N > 1$ indicate that garnet is a residual phase in the source. Also depletion of HFSEs, such as Nb and Ti, implies the presence of refractory residual phases, such as rutile and titanite and amphibole in the source (Rapp, Shimizu, & Norman, 2003). The La/Sm vs. Sm/Yb diagram reflects the presence of amphibole, garnet, and pyroxene in the origin of these magmatic rocks (Figure 11a). Amphiboles in these rocks are in the array of pargasitic to hastingsitic hornblende. Based on Thomas (1982) and Holloway (1973), pargasitic–hastingsitic hornblende in calc-alkalic magmas are stable to considerably higher temperatures and pressures than alkali-poor amphiboles. In these hornblendes, the phenomenon of opacity is observed. According to Middlemost (1986), this opacity phenomenon is due to the presence of hydrous minerals moving into a less hydrous or anhydrous environment, that is, where clinopyroxene might stabilize at lower lithostatic pressure and (or) lower $P(H_2O)$. However, Rutherford and Devine (2003) attributed this phenomenon to a rapid drop in pressure, so opacity in amphibole may be related to a thermal or pressure quench. According to Faure (1986), magma within islands arc and along the continental margin tectonic settings is created by melting the following materials: (a) Oceanic crust that endured hydrothermal alteration, (b) Clastic sediments on the oceanic lithosphere, (c) Upper mantle of subduction regions, and (d) Rocks in continental crust or at the base of the volcanic peaks of the arcs. Nicholson, Black, Hoskin, and Smith (2004) considered that enrichment in LREE and LILE to HREE and HFSE is one of the important properties in continental arcs in regions of subduction. Based on the diagrams of P_2O_5 and TiO_2 vs. SiO_2 (Wang et al., 2004, 2006), the adakitic rocks plot along the subducted oceanic crust-derived adakite array. Only a few examples of felsic rocks in the southern part of the Sabzevar fall into the field of thick lower crust-derived adakites.

5.2 | Tectonic setting and geodynamics evolution

Based on Wakabayashi and Shervais (2012) and Shervais et al. (2019), subduction is an event in the convergent margin and it is one of the main pillars for existing tectonic plates. The total geochemical and isotopic data obtained from the studied rock samples indicate that: these HSA magmas were derived from the melting of the hydrothermally altered oceanic lithosphere that was subducted, possibly along with the subducted sediments. In contrast, the lower silica adakites (LSA) were formed by melting of the mantle wedge, which has been transformed (metasomatized) by fluids released from the hydrous subducting oceanic slab. Lucci et al. (2016) and Verdel et al. (2011) attributed Eocene magmatism to decompression melting of the lithospheric mantle (suprasubduction zone metasomatism) hydrated by fluids released from the downgoing Tethyan oceanic crustal slab. In the model presented by Moyen (2009), HSAs are produced by melting oceanic lithosphere at a depth of about 70 km in amphibolite or eclogite facies conditions and LSAs are produced by melting of metasomatized mantle above the subducted oceanic slab at depths of 50 to 60 km. According to an investigation that was done by Rossetti et al. (2014) on thermobarometry of adakite rocks in the Sabzevar region, the presence of high-pressure amphibolite to granulite has been confirmed. Under these conditions, the garnet remains a stable phase.

The closing of the Palaeo-Tethys Ocean and opening the Neo-Tethys Ocean has led to many tectonic events in Iran. The movement to the north of the Arabic Plate during the Triassic-Jurassic leads to the subduction of the Neo-Tethys Ocean beneath Central Iran. The sub-continental lithospheric mantle (SCLM) below central Iran is recognized to be thin on a regional-scale, as is noted for Turkey (Hafkenscheid, Wortel, & Spakman, 2006; Omrani et al., 2008).

There is a prolonged debate over the initial timing of the resultant collision and continental shortening. This collision between two plates resulted in numerous magmatic events in the CISZ (Yousefi, Sadeghian, Samyari, & Ghasemi, 2017). These volcanic and intrusive rocks in this region of the CISZ are definitely the result of subduction of Neo-Tethys Ocean (Sabzevar branch) and the post-Eocene magmatism that occurred in the Oligocene to Miocene (Asiabanha & Foden, 2012; Ghasemi & Rezaei Kahkhaei, 2015; Jamshidi et al., 2015, 2018; Shabanian, Acocella, Gioncada, Ghasemi, &

Bellier, 2012; Yousefi et al., b). According to the ages obtained by U–Pb geochronology, these hypabyssal intrusive and volcanic rocks in Qouchan-Esfarayen magmatic belt have a lower age than the rocks of the other two adjacent regions. These magmatic belts are considered as the final magmatic event of subduction of the Neo-Tethys Oceanic lithosphere with U–Pb ages of 17.83 ± 0.24 Ma and 8.5 ± 0.3 Ma. According to Gardideh et al. (2018) and Spies, Lensch, and Mihm (1983) about a hundred million years ago, there was a branch of the active Neo-Tethys oceanic basin in the Qouchan area that closed in the Late Cretaceous to early Tertiary. In the Eocene volcano-sedimentary series had been deposited in this basin. Late Eocene–Oligocene orogenic movements trans-formed the Eocene marine system to an emergent continental set-ting; subsequently, magmatic activities of the Pyrenean orogenic phase, during the Oligocene–Miocene and Plio–Pleistocene, resulted in the formation of intermediate to acidic igneous rocks, such as andesitic-dacitic and basaltic flows.

In many of today's offshore near arc environments where signifi-cant amounts of sediment are deposited upon oceanic crust pelagically and within the trench setting, the Th/Yb in the lava is greater than two (Nebel et al., 2007), which reaches up to 10 in adakitic rocks of Qouchan-Esfarayen.

Although the age of some parts of the Qouchan-Esfarayen magmatism has been determined, further U–Pb zircon analyses yielded new important results. These new results were presented for the first time by Gardideh et al. (2018). It should be mentioned that the earliest magmatism associated with the subduction of the Neo-Tethys oceanic plate in this part of Iran is the magmatic belt of Torud-Ahmad Abad in south and southeast Shahrood with ages of 41.4 ± 0.3 Ma and 35.5 ± 0.2 Ma. Previously, it was mentioned that the Sabzevar magmatic region, with an age of approximately of 45 Ma, is adjacent to Torud-Ahmad Abad magmatic belt in south and southeast of Shahrood to the east and are very close to each other in terms of age. The age in Sabzevar region has also been confirmed by Shafaii Moghadam et al. (2016), although there is always debate about the age of geological events in these areas. Verdel et al. (2011) also presented ages between 54 and 37 Ma for the same rocks from central and northern parts of Iran. Based on these geochemical discrimination techniques and the radigenic isotopic results (Figure 10), the subduction of Neotethyan oceanic slab beneath the continental plate to form a magmatic arc is obvious.

The Neotethyan oceanic lithosphere may have broken off during subduction. Agard et al. (2011) suggested that the magmatism in this part of Iran may be related to break-off of the Neotethyan slab. Com-parison of these adakitic rocks with the studies conducted by Jamshidi et al. (2018), Gardideh et al. (2018), Shafaii Moghadam et al. (2015, 2016), Jamshidi et al. (2015), Lucci et al. (2016), and Rossetti et al. (2014) confirm the similar geochemical characteristics between the adakitic rocks in these regions. Common geochemical features have been reported between the adakitic rocks of west of Neyshabur (Tanha, 2009) and southwest of Birjand (Dehnavi, Shahri, & Sadeghian, 2009). The adakitic rocks in these areas have also been
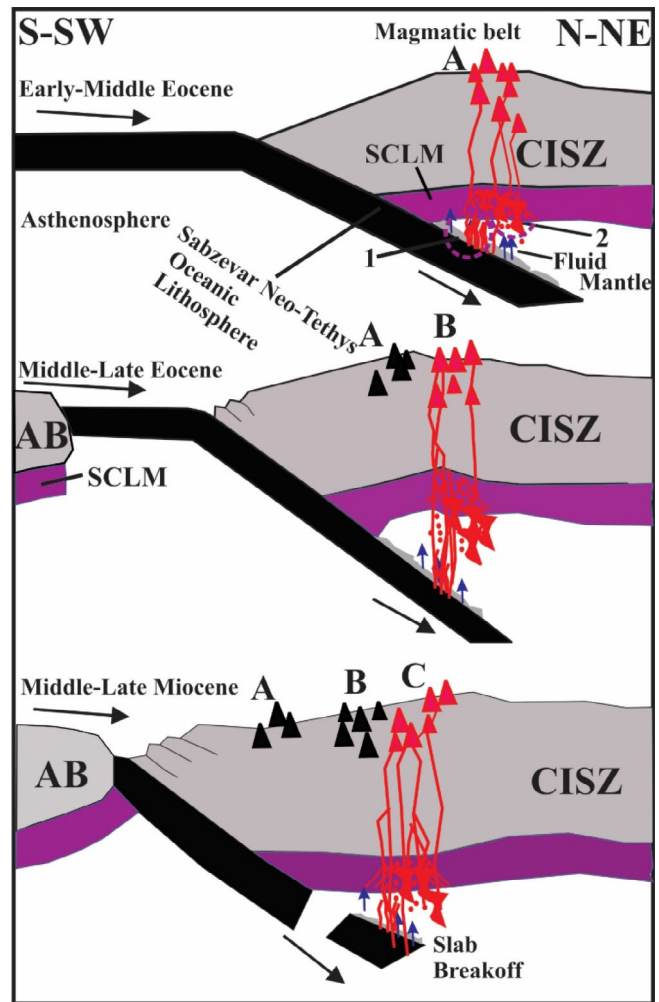

FIGURE 12 General schematic models (a–c) of a sequence of tectonic events, related to the sequential closure of the ocean basin (Neo-Tethys) via subduction with mantle-ocean crust interaction to enhance slab melting, in northern central Iran. AB: Arabian Plate. CISZ: Central Iran Structural Zone. SCLM: Subcontinental lithosphere mantle (uppermost solid mantle). (a) Rocks in south-southeast of Shahrood. (b) Rocks in Sabzevar area. (c) Rocks of Qouchan region. In this model, the subduction of the Neotethyan oceanic slab is seen below Central Iran Structural Zone. In this schematic illustration, two groups of rocks are shown, which are fully covered in the text 1: high silica adakite (HSA), 2: low silica adakite (LSA). In the final stages of subduction, the subducted oceanic crustal sheet is broken and parts of the separated plate are melted, which has contributed to the formation of the late magmatism. (All rocks are observed in the three zones, which are mentioned in the petrographic section). In this model, the active volcanic units in each period are shown in red and the existing units in the previous periods are shown in black [Colour figure can be viewed at wileyonlinelibrary.com]

affected by the subduction of ocean lithosphere and melting of meta-somatized mantle above the subducted oceanic slab. According to Shafaii Moghadam et al. (2016) and Lucci et al. (2016), Eocene adakitic rocks in northern Sabzevar in the area adjacent to the Torud-Ahmadabad Magmatic Belt are also the result of the subduction of the Neo-Tethys oceanic plate. According to their research, that

magmatic episode may be related to a flare up. Shafaii Moghadam et al. (2015, 2016) has mentioned that such magmas form under certain conditions, including: (a) subduction of young, hot downgoing slab; (b) slab breakoff in a post–collisional setting; (c) slab window processes related to ridge subduction; (c) partial melting of thickened continental lower crust, and (e) hydrous (involving amphibole) and (or) high pressure (involving garnet) crystal fractionation of a parent mafic magma. Then Lucci et al. (2016) suggested that a magmatic flare-up event is recognized during Eocene times, as documented by distribution of magmatic products both along the collisional zone and intraplate domains of Central Iran. According to all available studies and data about this region of Iran, we suggest that during the closure of the Middle Eocene sedimentary-volcanic basin, locally, subduction of the Neo-Tethys oceanic plate (Sabzevar branch) continues into the mantle. If subduction continues, evidence of continental margin magmatism and locally extension is clear. Transpression can cause slab windows, slab rollback, and slab breakoff that also can induce asthenosphere upwelling, in addition to SCLM and crustal local extension (leading to voluminous magmatism). In other words, transpression (locally extensional) aids in slab melting and migration through the cooled (refrigerated) suprasubduction zone mantle then SCLM and crust. Based on field observations, geochemistry, and isotopic data, we present a series of summary schematic figures to illustrate the continued subduction of the Neo-Tethys oceanic plate (Figure 12). It is likely that in the final stages of subduction, the oceanic plate broken off (slab failure), such that this failed segment section played an important role in the formation of the voluminous Qouchan-Esfarayen magmatism.

6 | CONCLUSIONS

The volcanic and intrusive rocks in the northern part of the CISZ are trachybasaltic andesite, andesite, trachyandesite, trachyte, dacite, and rhyolite. Based on geochemical studies, these rocks have adakite and adakite-like signatures. In rocks with high Sr/Y, the silica content varies between 51 and 63 wt% in Torud-Ahmad Abad magmatic rocks, Na_2O content is >3 wt%, and Al_2O_3 content is >16 wt%, with Yb is <1.8 ppm and Y is <18 ppm. Based on all field evidence, geochemistry, and tracer radiogenic isotopes, specifically the primitive Sr and Nd results noted in this review, these volcanic and intrusive rocks in the northern part of the CISZ are definitely the result of arc-like magmatism associated with subduction of Neo-Tethys oceanic lithosphere (Sabzevar branch) to amphibolite to eclogite facies and resultant late- to post-Eocene magmatism that happened from the Late Eocene into the Miocene.

The age of the magmatic belt in three areas of Qouchan-Esfarayen, south to southeast of Shahrood and Sabzevar is 17.83 ± 0.24 to 8.50 ± 0.34 Ma, 41.4 ± 0.3 to 35.5 ± 0.2 Ma, and 45 Ma, respectively. These robust U–Pb geochronologic results strongly support the relationship with convergent margin magmatism, emphasizing synchronous subduction of Neo-Tethys altered oceanic lithosphere. The hypabyssal adakitic rocks in Torud-Ahmad Abad region depend on the initiation of oceanic plate subduction. With the continuation of subduction-related magmatism, the hypabyssal intrusive and volcanic rocks of the Sabzevar area are emplaced and at the terminal phase of this subduction (closure of Neo-Tethys), the igneous rocks in Qouchan-Esfarayn were produced. According to the all currently available information, the HSAs are produced by melting altered upper oceanic lithosphere and LSAs were generated by melting of metasomatized suprasubduction zone mantle above the descending hot subducting altered oceanic slab.

CONFLICT OF INTEREST

The authors declare no conflict of interest.

PEER REVIEW

The peer review history for this article is available at https://publons.com/publon/10.1002/gj.3943.

ORCID

Fazilat Yousefi (iD) https://orcid.org/0000-0001-6081-790X

REFERENCES

Aftabi, A., & Atapour, H. (2009). Comments on "Arc magmatism and subduction history beneath the Zagros Mountains, Iran." In: A new report of adakites and geodynamic consequences by J. Omrani, P. Agard, H. Whitechurch, M. Bennoit, G. Prouteau, L. Jolivet. *Lithos*, *113*(3–4), 844–846. https://doi.org/10.1016/j.lithos.2008.09.008.

Agard, P., Omrani, H., Jolivet, L., Whitechurch, H., Vrielynck, B., Spakman, W., … Wortel, R. (2011). Zagros orogeny: A subduction-dominated process. *Geological Magazine*, *148*, 692–725. https://doi.org/10.1017/S001675681100046X.

Allen, M. B., & Armstrong, H. A. (2008). Arabia-Eurasia collision and the forcing of mid Cenozoic global cooling. *Palaeogeography, Palaeoclimatology, Palaeoecology*, *265*, 52–58. https://doi.org/10.1016/j.palaeo.2008.04.021.

Asiabanha, A., & Foden, J. (2012). Post-collisional transition from an extensional volcano-sedimentary basin to a continental arc in the Alborz Ranges, N-Iran. *Lithos*, *148*, 98–111. https://doi.org/10.1016/j.lithos.2012.05.014.

Azer, M. K. (2007). Tectonic significance of Late Precambrian calc-alkaline and alkaline magmatism in Saint Katherina area, southern Sinai, Egypt. Geologica Acta: An international earth science. *Journal*, *5*(3), 255–272. https://doi.org/10.1344/105.000000298.

Balaghi Einalou, M., Sadeghian, M., Minggou, Z., Ghasemi, H., & Mohajjel, M. (2014). Zircon U–Pb ages, Hf isotopes and geochemistry of the schists, gneisses and granites in Delbar Metamorphic-Igneous Complex, SE of Shahrood (Iran): Implications for Neoproterozoic geodynamic evolutions of Central Iran. *Journal of Asian Earth Sciences*, *92*, 92–124. https://doi.org/10.1016/j.jseaes.2014.06.011.

Berberian, F., & Berberian, M. (1981). Tectono-Plutonic episodes in Iran. *Geological Survey of Iran*, *Rep52*, 566–593. https://doi.org/10.1029/GD003p0005.

Berberian, F., & King, G. C. P. (1981). Towards a Paleogeography and tectonic evolution of Iran. *Canadian Journal of Earth Sciences*, *5*, 101–117. https://doi.org/10.1139/e81-019.

Blundy, J. D., & Shimizu, N. (1991). Trace element evidence for plagioclase recycling in calc-alkaline magmas. *Earth and Planetary Science Letters*, *102*, 178–197. https://doi.org/10.1016/0012-821X(91)90007-5.

Castillo, P. R. (2008). Origin of the adakite-high-Nb basalt association and its implications for post-subduction magmatism in Baja California, Mexico. *Geological Society of America Bulletin*, *120*, 451–462. https://doi.org/10.1130/B26166.1.

Castillo, P. R. (2012). Adakite petrogenesis. *Lithos*, *134–135*, 304–316. https://doi.org/10.1016/j.lithos.2011.09.013.

Chen, S., Niu, Y., Li, J., Sun, W., Zhang, Y., Hu, Y., & Shao, F. (2016). Syn-collisional adakitic granodiorites formed by fractional crystallization: Insights from their enclosed mafic magmatic enclaves (MMEs) in the Qumushan pluton, North Qilian Orogen at the northern margin of the Tibetan Plateau. *Lithos*, *248*, 455–468. https://doi.org/10.1016/j.lithos.2016.01.033.

Chiaradia, M. (2015). Crustal thickness control on Sr/Y signatures of recent arc magmas: An Earth scale perspective. *Scientific Reports*, *5* (8115), 1–5. https://doi.org/10.1038/srep08115.

Defant, M. J., & Drummond, M. S. (1990). Derivation of some modern arc magmas by melting of young subducted lithosphere. *Nature*, *347*, 662–665. https://doi.org/10.1038/347662a0.

Defant, M. J., Richerson, M., De Boer, J. Z., Stewart, R. H., Maury, R. C., Bellon, H., … Jackson, T. E. (1991). Dacite genesis via both slab melting and differentiation: Petrogenesis of La Yeguada volcanic complex, Panama. *Journal of Petrology*, *32*, 1101–1142. https://doi.org/10.1093/petrology/32.6.1101.

Dehnavi, N. Kh., Shahri M. h., & Sadeghian, M. (2009). Petrology and Geochemistry of subvolcanic of City of Firoozeh Neyshabour in west of Neyshabour. Paper presented at Articles of the 12th Iranian Geological Society Conference, Ahvaz - National Company of Southern Oil Fields, 1844–1848 (In Persian with English abstract).

Deng, C., Sun, G., Sun, D., Huang, H., Zhang, J., & Gou, J. (2017). Origin of C type adakite magmas in the NE Xing'an block, NE China and tectonic implication. *Acta Geochimica*, *37*, 281–294. https://doi.org/10.1007/s11631-017-0190-2.

Drake, M. J., & Weill, D. F. (1975). Partition of Sr, Ba, Ca, Y, Eu2+, Eu3+, and other REE between plagioclase feldspar and magmatic liquid: An experimental study. *Geochimica et Cosmochimica Acta*, *39*(5), 689–712.

du Bray, E. A. (2017). Geochemical characteristics of igneous rocks associated with epithermal mineral deposits—a review. *Ore Geology Reviews*, *80*, 767–783. https://doi.org/10.1016/j.oregeorev.2016.08.023.

Eyuboglu, Y., Chung, S. L., Santosh, M., Dudas, F. O., & Akaryal, E. (2011). Transition from shoshonitic to adakitic magmatism in the eastern Pontides, NE Turkey: Implications for slab window melting. *Gondwana Research*, *19*, 413–429. https://doi.org/10.1016/j.gr.2010.07.006.

Eyuboglu, Y., Santosh, M., & Chung, S. L. (2011). Petrochemistry and U-Pb zircon ages of adakitic intrusions from the Pulur Massif (Eastern Pontides, NE Turkey): Implications for slab rollback and ridge subduction associated with Cenozoic convergent tectonics in the Eastern Mediterranean. *Journal of Geology*, *119*, 394–417. https://doi.org/10.1086/660158.

Eyuboglu, Y., Santosh, M., Yi, K., Bektaş, O., & Kwon, S. (2012). Discovery of Miocene adakitic dacite from the Eastern Pontides Belt (NE Turkey) and a revised geodynamic model for the Late Cenozoic evolution of the Eastern Mediterranean region. *Lithos*, *146-147*, 218–232. https://doi.org/10.1016/j.lithos.2012.04.034.

Faure, G. (1986). *Principles of isotope geology* (2nd ed.), 589 pp. New York, NY: Wiley. https://trove.nla.gov.au/version/45658412.

Fu, F. Q., McInnes, B. I. A., Evans, N. J., & Davies, P. J. (2010). Numerical modeling of magmatic–hydrothermal systems constrained by U–Th–Pb–He time–temperature histories. *Journal of Geochemical Exploration*, *106*, 90–109. https://doi.org/10.1016/j.gexplo.2009.09.001.

Gardideh, S., Ghasemi, H., & Sadeghian, M. (2018). The age of U–Pb on zircon crystals, isotope ratio of Rb–Sr and geochemistry of Neogene adakite of magmatism domes of Qouchan-Esfarayn, northeast of Iran. *Iranian Journal of Crystallography and Mineralogy*, *2*, 455–478 (In Persian with English abstract).

Ghasemi, H., & Rezaei Kahkhaei, M. (2015). Petrochemistry and tectonic setting of the Davarzan Abbas Abad Eocene Volcanic (DAEV) rocks, NE Iran. *Journal of Mineralogy and Petrology*, *6*, 235–252. https://doi.org/10.1007/s00710-014-0353-3.

Guan, Q., Zhu, D. C., Zhao, Z. D., Zhang, L. L., Liu, M., Li, X. W., … Mo, X. X. (2010). Late Cretaceous adakites from the eastern segment of the Gangdese Belt, Southern Tibet: Products of Neo-Tethyan mid-ocean ridge subduction. *Acta Petrologica Sinica*, *26*, 2165–2179 (In Chinese with English abstract).

Guest, B., Horton, B. K., Axen, G. J., Hassanzadeh, J., & McIntosh, W. C. (2007). Middle to Late Cenozoic basin evolution in the western Alborz Mountains: Implications for the onset of collisional deformation in northern Iran. *Tectonics*, *26*, TC6011. https://doi.org/10.1029/2006TC002091.

Hafkenscheid, E., Wortel, M. J. R., & Spakman, W. (2006). Subduction history of the Tethyan derived seismic tomography and tectonic reconstruction. *Tectonics*, *111*, 1–26 https://0148-0227/06/2005JB003791$09.00.

Haghipour, A. A., & Aghanabati, S. A. (1985). Geological Map of Iran. *Geological Survey of Iran*.

Han, B. F., Wang, S. G., Jahn, B. M., Hong, D. W., Kagami, H., & Sun, Y. L. (1997). Depleted-mantle source for the Ulungur River A-type granites from North Xinjiang, China: Geochemistry and Nd–Sr isotopic evidence, and implications for Phanerozoic crustal growth. *Chemical Geology*, *138* (3–4), 135–159. https://doi.org/10.1016/S0009-2541(97)00003-X.

Harker, A. (1909). *The natural history of igneous rocks*. London, UK: Methuen and Co.

Harvey, J., & Baxter, E. F. (2009). An improved method for TIMS high precision neodymium isotope analysis of very small aliquots (1–10 ng). *Chemical Geology*, *258*, 251–257. https://doi.org/10.1016/j.chemgeo.2008.10.024.

Haschke, M. R., & Ben-Avraham, Z. (2005). Adakites from collision-modified lithosphere. *Geophysical Research Letters*, *32*, 1–4. https://doi.org/10.1029/2005GL023468.

Holloway, J. R. (1973). The system pargasite–H_2O–CO_2: A model for melting of a hydrous mineral with a mixed-volatile fluid—I. Experimental results to 8 kbar. *Geochimica et Cosmochimica Acta*, *37*, 651–666. https://doi.org/10.1016/0016-7037(73)90225-1.

Hosseini, S. H., Sadeghian, M., Minggou, Z., & Ghasemi, H. (2015). Petrology, geochemistry and zircon U–Pb dating of Band-e-Hezarchah metabasites (NE Iran): An evidence for back-arc magmatism along the northern active margin of Gondwana. *Chemie der Erde*, *75*, 207–219. https://doi.org/10.1016/j.chemer.2015.02.002.

Jamshidi, K., Ghasemi, H., Miao, L., & Sadeghian, M. (2018). Adakite magmatism within the Sabzevar ophiolite zone, NE Iran: U–Pb geochronology and Sr–Nd isotopic evidences. *Geopersia*, *8*, 111–130. https://doi.org/10.22059/geope.2017.242944.648352.

Jamshidi, K., Ghasemi, H., Troll, V. R., Sadeghian, M., & Dahren, B. (2015). Magma storage and plumbing of adakite-type post-ophiolite intrusion in the Sabzevar ophiolitic zone, northern Iran. *Solid Earth*, *6*, 49–72. https://doi.org/10.5194/se-6-49-2015.

John, T., Klemd, R., Klemme, S., Elis Hoffmann, J., & Gao, J. (2011). Nb–Ta fractionation by partial melting at the titanite–rutile transition. *Contributions to Mineralogy and Petrology*, *161*, 35–45. https://doi.org/10.1007/s00410-010-0520-4.

Kay, R. H. (1978). Aleutian magnesian andesites: Melts from subducted Pacific Ocean crust. *Journal of Volcanology and Geothermal Research*, *4*, 117–132. https://doi.org/10.1016/0377-0273(78)90032-X.

Kolb, M., Von Quadt, A., Peytcheva, I., Heinrich, C. A., Fowler, S. J., & Cvetkovic, V. (2013). Adakite-like and normal arc magmas: Distinct fractionation paths in the East Serbian Segment of the Balkan-Carpathian Arc. *Journal of Petrology*, *54*, 421–451. https://doi.org/10.1093/petrology/egs072.

Le Bas, M. J., Le Maitre, R. W., Streckeisen, A., & Zanettin, B. (1986). A chemical classification of volcanic rocks based on the total alkali-silica diagram. *Journal of Petrology*, *27*, 745–750. https://doi.org/10.1093/petrology/27.3.745.

Lucci, F., Rossetti, F., White, J. C., Moghadam, H. S., Shirzadi, A., & Nasrabady, M. (2016). Tschermak fractionation in calc-alkaline magmas: the Eocene Sabzevar volcanism (NE Iran). *Arabian Journal of Geosciences*, *9*(10), 573.

Lundblad, S. P. (1995). *Evolution of small carbonate platforms in the Umbria-Marche Apennines, Italy*.

Ma, Q., Zheng, J. P., Xu, Y. G., Griffin, W. L., & Zhang, R. S. (2015). Are continental "adakites" derived from thickened or foundered lower crust? *Earth and Planetary Science Letters*, *419*, 125–133. https://doi.org/10.1016/j.epsl.2015.02.036.

Macpherson, C. G., Dreher, S. T., & Thirlwall, M. F. (2006). Adakites without slab melting: high pressure differentiation of Island arc magma, Mindanao, The Philippines. *Earth and Planetary Science Letters*, *243*, 581–593. https://doi.org/10.1016/j.epsl.2005.12.034.

Maghdour-Mashhour, R., Esmaeily, D., Shabani, A. A. T., Chiaradia, M., & Latypov, R. (2015). Petrology and geochemistry of the Karaj Dam basement sill: Implications for geodynamic evolution of the Alborz magmatic belt. *Chemie der Erde-Geochemistry*, *75*(2), 237–260. https://doi.org/10.1016/j.chemer.2015.03.001.

Mahmoudi Nia, H., Baghban, S., & Simmonds, V. (2017). Geology, geochemistry and petrogenesis of post-collisional adakitic intrusions and related dikes in the Khoyanarood area, NW Iran. *Chemie der Erde*, *77*, 53–67. https://doi.org/10.1016/j.chemer.2017.02.001.

Maniar, P. D., & Piccoli, P. M. (1989). Tectonic discrimination of granitoids. *Geological Society of America Bulletin*, *101*, 635–643. https://doi.org/10.1130/0016-7606(1989)101<0635:TDOG>2.3.CO;2.

Martin, H., Smithies, R. H., Rapp, R., Moyen, J. F., & Champion, D. (2005). An overview of adakite, tonalite-trondhjemite-granodiorite (TTG), and sanukitoid: relationships and some implications for crustal evolution. *Lithos*, *79*, 1–24. https://doi.org/10.1016/j.lithos.2004.04.048.

Maruyama, S. (1997). Pacific-type orogeny revisited: Miyashiro-type orogeny proposed. *Island Arc*, *6*, 91–120. https://doi.org/10.1111/j.1440-1738.1997.tb00042.x.

Middlemost, E. A. (1986). *Magmas and magmatic rocks: An introduction to igneous petrology*, 266 pp. London & New York: Addison-Wesley Longman. https://doi.org/10.1180/minmag.1986.050.355.34.

Mohajjel, M., Fergusson, C. L., & Sahandi, M. R. (2003). Cretaceous-Tertiary convergence and continental collision Sanandaj-Sirjan zone Western Iran. *International Journal of Earth Sciences*, *21*, 397–412. https://doi.org/10.1016/S1367-9120(02)00035-4.

Molinaro, M., Zeyen, H., & Laurencin, X. (2005). Lithospheric structure beneath the south-eastern Zagros Mountains, Iran: Recent slab break-off? *Terra Nova*, *17*(1), 1–6. https://doi.org/10.1111/j.1365-3121.2004.00575.x.

Moyen, J. F. (2009). High Sr/Y and La/Yb ratios: The meaning of the "adakitic signature". *Lithos*, *112*, 556–574. https://doi.org/10.1016/j.lithos.2009.04.001.

Moyen, J. F., & Stevens, G. (2006). Experimental constraints on TTG petrogenesis: Implications for Archean geodynamics. *Geophysical Monograph*, *164*, 149–175. https://doi.org/10.1029/164GM11.

Müller, D., & Groves, D. I. (1993). Direct and indirect associations between potassic igneous rocks, shoshonites and gold–copper deposits. *Ore Geology Reviews*, *8*, 383–406. https://doi.org/10.1016/0169-1368(93)90035-W.

Murphy, J. B. (2007). Arc-magmatism II: Geochemical and isotopic characteristics. *Geoscience Canada*, *34*, 7–35.

Nakamura, H., & Iwamori, H. (2013). Generation of adakites in a cold subduction zone due to double subducting plates. *Contributions to Mineralogy and Petrology*, *165*, 1107–1134. https://doi.org/10.1007/s00410-013-0850-0.

Nakamura, N. (1974). Determination of REE, Ba, Fe, Mg, Na and K in carbonaceous and ordinary chondrites. *Geochimica et Cosmochimica Acta*, *38*, 757–775. https://doi.org/10.1016/0016-7037(74)90149-5.

Nebel, O., Münker, C., Nebel-Jacobsen, Y. J., Kleine, T., Mezger, K., & Mortimer, N. (2007). Hf–Nd–Pb isotope evidence from Permian arc rocks for the long-term presence of the Indian–Pacific mantle boundary in the SW Pacific. *Earth and Planetary Science Letters*, *254*(3–4), 377–392.

Nicholson, K. N., Black, P. M., Hoskin, P. W. O., & Smith, I. E. M. (2004). Silicic volcanism and back arc extension related to migration of the Late CenozoicAustralian-Pacific plate boundary. *Journal of Volcanology and Geothermal Research*, *131*, 295–306. https://doi.org/10.1016/S0377-0273(03)00382-2.

Omrani, J., Agard, P., Whitechurch, H., Benoit, M., Prouteau, G., & Jolivet, L. (2008). Arc-magmatism and subduction history beneath the Zagros Mountains, Iran: A new report of adakites and geodynamic consequences. *Lithos*, *106*(3–4), 380–398. https://doi.org/10.1016/j.lithos.2008.09.008.

Pearce, J. A. (1983). Role of the sub-continental lithosphere in magma genesis at active continental margins. In C. J. Hawkesworth & M. J. Norry (Eds.), *Continental basalts and Mantle Xenoliths* (pp. 230–249). Cheshire, UK: Shiva Publishing https://orca.cf.ac.uk/id/eprint/8626.

Pearce, J. A. (2014). Immobile element fingerprinting of ophiolites. *Elements*, *10*, 101–108. https://doi.org/10.2113/gselements.10.2.101.

Peccerillo, A., & Taylor, S. R. (1976). Geochemistry of Eocene calc-alkaline volcanic rocks from the Kastamonu area, northern Turkey. *Contributions to Mineralogy and Petrology*, *58*, 63–81. https://doi.org/10.12691/jgg-6-2-4.

Rapp, R. P., Shimizu, N., & Norman, M. D. (2003). Growth of early continental crust by partial melting of eclogite. *Nature*, *425*, 605–609. https://doi.org/10.1038/nature02031.

Rapp, R. P., Shimizu, N., Norman, M. D., & Applegate, G. S. (1999). Reaction between slabderived melts and peridotite in the mantle wedge: Experimental constraints at 3.8 GPa. *Chemical Geology*, *160*, 335–356. https://doi.org/10.1016/S0009-2541(99)00106-0.

Rezaei Kahkhaei, M., Taheri Sarteshnizi, A., Ghasemi, H., & Gardideh, S. (2018). Geochemistry and isotope geology of adakitic domes from Chakane area in South of Quchan (Northeast of Iran). *Journal of Petrology of Isfahan University, Iran*, *9*(36), 25–48 (In Persian with English abstract).

Ribeiro, J. M., Maury, R. C., & Grégoire, M. (2016). Are adakites slab melts or high-pressure fractionated mantle melts? *Journal of Petrology*, *57*(5), 839–862. https://doi.org/10.1093/petrology/egw023.

Richards, J. P., & Kerrich, R. (2007). Adakite-like rocks: Their diverse origins and questionable role in metallogenesis. *Economic Geology*, *102*, 537–576. https://doi.org/10.2113/gsecongeo.102.4.537.

Richards, J. P., Spell, T., Rameh, E., Razique, A., & Fletcher, T. (2012). High Sr/Y magmas reflect arc maturity, high magmatic water content, and porphyry Cu ± Mo ± Au potential: Examples from the Tethyan Arcs of central and eastern Iran and Western Pakistan. *Economic Geology*, *107*, 295–332. https://doi.org/10.2113/econgeo.107.2.295.

Ringwood, A. E. (1990). Slab-mantle interactions. 3. Petrogenesis of intraplate magmas and structure of the upper mantle. *Chemical Geology*, *82*, 187–207. https://doi.org/10.1016/0009-2541(90)90081-H.

Rollinson, H. R. (1993). *Using geochemical data: Evaluation, presentation, interpretation*, 325 pp. London, UK: Routledge, Taylor and Francis Group.

Rossetti, F., Nasrabady, M., Theye, T., Gerdes, A., Monie, P., Lucci, F., & Vignaroli, G. (2014). Adakite differentiation and emplacement in a subduction channel: The Late Paleocene Sabzevar magmatism (NE Iran).

Geological Society of America Bulletin, *126*, 317–343. https://doi.org/10.1130/B30913.1.

Rutherford, M. J., & Devine, A. D. (2003). Magmatic conditions and magma ascent as indicated by horn blende phase equilibria and reaction in the 1995–2002, Soufriere Hills magma. *Journal of Petrology*, *44*, 1433–1484. https://doi.org/10.1093/petrology/44.8.1433.

Sengor, A. M. C., & Kidd, W. S. F. (1979). Post-collisional tectonics of the Turkish–Iranian plateau and a comparison with Tibet. *Tectonophysics*, *55*, 361–376. https://doi.org/10.1016/0040-1951(79)90184-7.

Shabanian, E., Acocella, V., Gioncada, A., Ghasemi, H., & Bellier, O. (2012). Structural control on volcanism in intraplate post collisional settings: Late Cenozoic to Quaternary examples of Iran and Eastern Turkey. *Tectonics*, *31*, 3013–3042. https://doi.org/10.1029/2011TC003042.

Shafaii Moghadam, H., Li, X. H., Ling, X. X., Santos, J. F., Stern, R. J., Li, Q. L., & Ghorbani, G. (2015). Eocene Kashmar granitoids (NE Iran): Petrogenetic constraints from U–Pb zircon geochronology and isotope geochemistry. *Lithos*, *216*, 118–135.

Shafaii Moghadam, H., Rossetti, F., Lucci, F., Chiaradia, M., Gerdes, A., Martinez, M. L., … Nasrabady, M. (2016). The calc-alkaline and adakitic volcanism of the Sabzevar structural zone (NE Iran): Implications for the Eocene magmatic flare-up in Central Iran. *Lithos*, *248-251*, 517–535. https://doi.org/10.1016/j.lithos.2016.01.019.

Shafiei, S., Haschke, M., & Shahabpour, J. (2009). Recycling of orogenic arc crust triggers porphyry Cu mineralization in Kerman Cenozoic arc rocks, southeastern Iran. *Mineralium Deposita*, *44*, 265–283. https://doi.org/10.1007/s00126-008-0216-0.

Shahabpour, J. (2007). Island-arc affinity of the Central Iranian volcanic belt. *International Journal of Asian Earth Sciences*, *30*, 652–665. https://doi.org/10.1016/j.jseaes.2007.02.004.

Shervais, J. W., Reagan, M., Haugen, E., Almeev, R. R., Pearce, J. A., Prytulak, J., … Vetter, S. K. (2019). Magmatic response to subduction initiation: Part 1. Fore-arc basalts of the Izu-Bonin Arc from IODP Expedition 352. *Geochemistry, Geophysics, Geosystems*, *20*, 1–26. https://doi.org/10.1029/2018GC007731.

Simmonds, V. (2013). Geochemistry and petrogenesis of an adakitic quartz-monzonitic porphyry stock and related cross-cutting dike suites, Kighal, northwest Iran. *International Geology Review*, *55*(9), 1126–1144. https://doi.org/10.1080/00206814.2013.767491.

Spies, O., Lensch, G., & Mihm, A. (1983). Geochemistry of the post-ophiolitic Tertiary volcanics between Sabzevar and Quchan (NW Iran). Geodynamic project (Geotraverse) in Iran. *Geological Survey of Iran Report*, *51*, 264–289.

Stampfli, G. M., & Borel, G. D. (2002). A plate tectonic model for the Paleozoic and Mesozoic constrained by dynamic plate boundaries and restored synthetic oceanic isochrones. *Earth and Planetary Science Letters*, *196*, 17–33. https://doi.org/10.1016/S0012-821X(01)00588-X.

Stern, R. J., & Scholl, D. W. (2010). Yin and Yang of continental crust creation and destruction by plate tectonic processes. *International Geology Review*, *52*, 1–31. https://doi.org/10.1080/00206810903332322.

Stocklin, J. (1968). Structural history and tectonics of Iran: A review. *AAPG Bulletin*, *52*, 1229–1258.

Sun, S. S., & McDonough, W. F. (1989). Chemical and isotopic systematics of oceanic of basalts: implication for mantle composition and processes. In A. D. Saunders & M. J. Norry (Eds.), *Magmatism in oceanic basins* (Vol. 42, pp. 313–345). Geological Society London Special Publications. https://doi.org/10.1144/GSL.SP.1989.042.01.19.

Tanha, A. (2009). *Petrogenesis of Neogene igneous rocks in the north of Anbarabad (Meshkan)*. M.S. thesis, Shahrood University of Technology, 150 pp. (In Persian with English abstract).

Temizel, E. (2014). Petrochemical evidence of magma mingling and mixing in the Tertiary monzogabbroic stocks around the Bafra (Samsun) area in Turkey: Implications of coeval mafic and felsic magma interactions. *Mineralogy and Petrology*, *108*, 353–370. https://doi.org/10.1007/s00710-013-0304-4.

Temizel, I., Arslan, M., Ruffet, G., & Peucat, J. J. (2012). Petrochemistry, geochronology and Sr–Nd isotopic systematics of the Tertiary collisional and post-collisional volcanic rocks from the Ulubey (Ordu) area, eastern Pontide, NE Turkey: Implication for extension-related origin and mantle source characteristic. *Lithos*, *128*, 126–147. https://doi.org/10.1016/j.lithos.2011.10.006.

Temizel, I., Arslan, M., Yücel, C., Abdioğlu, E., & Ruffet, G. (2016). Geochronology and geochemistry of Eocene-aged volcanic rocks around the Bafra (Samsun, N Turkey) area: Constraints for the interaction of lithospheric mantle and crustal melts. *Lithos*, *258*, 92–114. https://doi.org/10.1016/j.lithos.2016.04.023.

Thomas, W. M. (1982). Stability relations of the amphibole hasting site. *American Journal of Science*, *282*, 136–164. https://doi.org/10.2475/ajs.282.2.136.

Verdel, C., Wernicke, B. P., Hassanzadeh, J., & Guest, B. (2011). A Paleogene extensional arc flare-up in Iran. *Tectonics*, *30*, 20. https://doi.org/10.1029/2010TC002809.

Vernon, R. H. (2008). *A practical guide to rock microstructure*, 579 pp. Cambridge, United Kingdom: Cambridge University Press.

Wakabayashi, J., & Shervais, J. W. (2012). Introduction: Initiation and termination of subduction—Rock record, geodynamic models, and modern plate boundaries. *Lithosphere*, *4*(6), 467–468. https://doi.org/10.1130/LINT1.1.

Wang, Q., Wyman, D. A., Xu, J.-F., Zhao, Z. H., Jian, P., Xiong, X. L., … Bai, Z. H. (2006). Petrogenesis of Cretaceous adakitic and shoshonitic igneous rocks in the Luzong area, Anhui Province (Eastern China): Implications for geodynamics and Cu–Au mineralization. *Lithos*, *89*, 424–446. https://doi.org/10.1016/j.lithos.2005.12.010.

Wang, Q., Xu, J. F., Zhao, Z. H., Bao, Z. W., Xu, W., & Xiong, X. L. (2004). Cretaceous high potassium intrusive rocks in the Yueshan-Hongzhen area of east China: Adakites in an extensional tectonic regime within a continent. *Geochemical Journal*, *38*, 417–434. https://doi.org/10.2343/geochemj.38.417.

Wang, Y. H., Zhang, F. F., Liu, J. J., & Que, C. Y. (2016). Carboniferous magmatism and mineralization in the area of the Fuxing Cu deposit, Eastern Tianshan, China: Evidence from zircon U–Pb ages, petrogeochemistry, and Sr–Nd–Hf–O isotopic compositions. *Gondwana Research*, *34*, 109–128. https://doi.org/10.1016/j.gr.2016.03.007.

Whitney, D. L., & Evans, B. W. (2010). Abbreviations for names of rock-forming minerals. *American Mineralogist*, *95*, 185–187. https://doi.org/10.2138/am.2010.3371.

Yousefi, F. (2017). *Petrogenesis and isotope geology of post Eocene intrusive rocks of Torud–Ahmad Abad magmatic belt (SE of Shahrood)*. PhD. thesis, Shahrood University of Technology, 247 pp. (In Persian with English abstract).

Yousefi, F., Papadopoulou, L., Sadeghian, M., Wanhainen, Ch., & Bark, G. (2019). Plagioclase hosted melt inclusion in hypabyssal rocks in Torud-Amad Abad magmatic belt. Paper presented at 15th International Congress of the Geological Society of Greece, Athens, 1–2.

Yousefi, F., Sadeghian, M., Wanhainen, C., Ghasemi, H., Lambrini, P., Bark, G., … Koroneos, A. (2017). Mineral chemistry and P-T conditions of the adakitic rocks from Torud–Ahmad Abad magmatic belt, S-SE Shahrood, NE Iran. *Journal of Geochemical Exploration*, *182*, 110–120. https://doi.org/10.1016/j.gexplo.2017.09.006.

Yousefi, F., Sadeghian, M., Wanhainen, C., Ghasemi, H., & Frei, D. (2017). Geochemistry, petrogenesis and tectonic setting of middle Eocene hypabyssal rocks of the Torud–Ahmad Abad magmatic belt: An implication for evolution of the northern branch of Neo-Tethys Ocean in Iran. *Journal of Geochemical Exploration*, *178*, 1–15. http://dx.doi.org/10.1016/j.gexplo.2017.03.008.

Zhu, A. C., Zhao, Z. D., Pan, G. T., Lee, H. Y., Kang, Z. Q., Liao, Z. L., … Liu, B. (2009). Early Cretaceous subduction-related adakite-like rocks

of the Gangdese Belt, southern Tibet: Products of slab melting and subsequent melt-peridotite interaction? *International Journal of Asian Earth Sciences*, *34*, 298–309. https://doi.org/10.1016/j.jseaes.2008.05.003.

SUPPORTING INFORMATION

Additional supporting information may be found online in the Supporting Information section at the end of this article.

How to cite this article: Yousefi F, Sadeghian M, Lentz DR, Wanhainen C, Mills RD. Petrology, petrogenesis, and geochronology review of the Cenozoic adakitic rocks of northeast Iran: Implications for evolution of the northern branch of Neo-Tethys. *Geological Journal*. 2020;1–18. https://doi.org/10.1002/gj.3943